Environmental Science Processes & Impacts

ROYAL SOCIETY OF CHEMISTRY

PAPER

View Article Online
View Journal

Cite this: DOI: 10.1039/d1em00260k

The Sea Spray Chemistry and Particle Evolution study (SeaSCAPE): overview and experimental methods†

Jon S. Sauer, ‡[a] Kathryn J. Mayer, ‡[a] Christopher Lee, ‡[b] Michael R. Alves,[a] Sarah Amiri,[bc] Cristina J. Bahaveolos,[d] Emily B. Franklin,[e] Daniel R. Crocker,[a] Duyen Dang,[a] Julie Dinasquet,[b] Lauren A. Garofalo,[f] Chathuri P. Kaluarachchi,[g] Delaney B. Kilgour,[d] Liora E. Mael,[a] Brock A. Mitts,[a] Daniel R. Moon,[hi] Alexia N. Moore,[a] Clare K. Morris,[b] Catherine A. Mullenmeister,[a] Chi-Min Ni,[d] Matthew A. Pendergraft,[b] Daniel Petras,[bj] Rebecca M. C. Simpson,[b] Stephanie Smith,[b] Paul R. Tumminello,[a] Joseph L. Walker,[b] Paul J. DeMott,[k] Delphine K. Farmer,[f] Allen H. Goldstein,[el] Vicki H. Grassian,[abm] Jules S. Jaffe,[b] Francesca Malfatti,[bn] Todd R. Martz,[b] Jonathan H. Slade,[a] Alexei V. Tivanski,[g] Timothy H. Bertram,[d] Christopher D. Cappa[h] and Kimberly A. Prather*[ab]

Marine aerosols strongly influence climate through their interactions with solar radiation and clouds. However, significant questions remain regarding the influences of biological activity and seawater chemistry on the flux, chemical composition, and climate-relevant properties of marine aerosols and gases. Wave channels, a traditional tool of physical oceanography, have been adapted for large-scale ocean-atmosphere mesocosm experiments in the laboratory. These experiments enable the study of aerosols under controlled conditions which isolate the marine system from atmospheric anthropogenic and terrestrial influences. Here, we present an overview of the 2019 Sea Spray Chemistry and Particle Evolution (SeaSCAPE) study, which was conducted in an 11 800 L wave channel which was modified to facilitate atmospheric measurements. The SeaSCAPE campaign sought to determine the influence of biological activity in seawater on the production of primary sea spray aerosols, volatile organic compounds (VOCs), and secondary marine aerosols. Notably, the SeaSCAPE experiment also focused on understanding how photooxidative aging processes transform the composition of marine aerosols. In addition to a broad range of aerosol, gas, and seawater measurements, we present key results which highlight the experimental capabilities during the campaign, including the phytoplankton bloom dynamics, VOC production, and the effects of photochemical aging on aerosol production, morphology, and chemical composition. Additionally, we discuss the modifications made to the wave channel to improve aerosol production and reduce background contamination, as well as subsequent characterization experiments. The SeaSCAPE experiment provides unique insight into the connections between marine biology, atmospheric chemistry, and climate-relevant aerosol properties, and demonstrates how an ocean-atmosphere-interaction facility can be used to isolate and study reactions in the marine atmosphere in the laboratory under more controlled conditions.

Received 2nd July 2021
Accepted 14th October 2021

DOI: 10.1039/d1em00260k

rsc.li/espi

[a]Department of Chemistry and Biochemistry, University of California, San Diego, La Jolla, California 92093, USA. E-mail: kprather@ucsd.edu
[b]Scripps Institution of Oceanography, University of California, San Diego, La Jolla, California 92093, USA
[c]Marine Science Institute, University of California, Santa Barbara, Santa Barbara, California 93106, USA
[d]Department of Chemistry, University of Wisconsin, Madison, Wisconsin 53706, USA
[e]Department of Civil and Environmental Engineering, University of California, Berkeley, California 94720, USA
[f]Department of Chemistry, Colorado State University, Fort Collins, Colorado 80523, USA
[g]Department of Chemistry, University of Iowa, Iowa City, Iowa 52242, USA
[h]Department of Civil and Environmental Engineering, University of California, Davis, California 95616, USA
[i]Institute for Chemical Science, Heriot-Watt University, Edinburgh EH14 4AS, UK
[j]Skaggs School of Pharmacy and Pharmaceutical Science, University of California, San Diego, La Jolla, California 92093, USA
[k]Department of Atmospheric Sciences, Colorado State University, Fort Collins, Colorado 80523, USA
[l]Department of Environmental Science, Policy and Management, University of California, Berkeley, California 94720, USA
[m]Department of Nanoengineering, University of California San Diego, La Jolla, California 92093, USA
[n]Universita' degli Studi di Trieste, Department of Life Sciences, Trieste, 34127, Italy

† Electronic supplementary information (ESI) available. See DOI: 10.1039/d1em00260k

‡ Authors contributed equally.

Environmental significance

The ocean-atmosphere system influences Earth's radiative balance, cloud formation and precipitation, and air quality, all of which directly impact human health and well-being. Laboratory control experiments play a key role in improving our understanding of the marine atmosphere and allow for measurements of aerosols and gases under clean, isolated, and environmentally relevant conditions. Here, we describe the design and operation of an 11 800 L wave channel for replicating the ocean-atmosphere environment, with specific details provided on the production of representative sea spray aerosols, marine microbiology, biogenic gases, and secondary marine aerosols. The findings presented herein demonstrate best experimentation practices and illustrate challenges that exist when working to replicate and ultimately understand chemical reactions and biology feedbacks in the ocean-atmosphere system.

1. Introduction

Oceans cover 71% of Earth's surface and are a major source of both aerosols and trace gases, which affect climate, air quality, and human health. Aerosols influence climate directly by absorbing and scattering solar radiation, and indirectly by serving as cloud condensation nuclei (CCN) and ice nucleating particles (INPs), thus affecting the properties of clouds. The interactions between aerosols and clouds represent one of the largest uncertainties in estimates of Earth's radiative budget.[1,2] Constraining the flux, composition, and cloud-relevant properties of marine aerosols is crucial for understanding their influence on atmospheric processes and establishing past and future changes in the climate system.

Sea spray aerosol (SSA) is the largest source of atmospheric particles by mass, with a global emission flux ranging from 3–30 Pg per year,[3] 98% of which is attributed to supermicron particles.[4] SSA is produced when breaking waves entrain air bubbles beneath the ocean surface, which rise to the surface and burst. This process produces two types of droplets: film drops from the bursting of the bubble cap and jet drops from the collapse of the bubble cavity.[3,5] Spume droplets can also be formed from the direct action of wind on wave crests; however, these large droplets (up to millimeters in diameter) are rapidly removed from the atmosphere *via* gravitational deposition.[3] Measurements of authentic marine aerosols have been traditionally limited to studies performed on research cruises or at remote field stations.[6,7] More recently, usage of ocean-atmosphere simulators such as wave channels and Marine Aerosol Reference Tanks (MARTs) have enabled laboratory studies to simulate the complexity of the marine environment under controlled conditions.[8–13] These experimental systems use breaking waves, plunging waterfalls, or plunging jets to produce bubble plumes with the correct size and surface residence time to match bubble distributions in the real ocean.[14,15] Subsequent rupturing of these bubbles at the air-sea interface produces SSA that closely resemble the size distribution of SSA observed in the marine environment.

These ocean-atmosphere simulators have been compared with other laboratory SSA production devices such as fritted bubblers and shown to have several key advantages.[9,10,16] While simple in design and application, fritted bubblers tend to produce less representative aerosol size distributions, resulting in physiochemical discrepancies in morphology and composition.[16] The use of ocean-atmosphere simulators to generate realistic marine aerosols has led to a variety of new insights into marine aerosol chemistry and production.[17] This includes the production of marine ice nucleating particles (INPs);[18] the aerosolization of marine microorganisms;[19] biochemical control of SSA composition;[20] biogenic volatile gas production;[21] physical and chemical heterogeneity of SSA;[22,23] and SSA surface reactivity and gas uptake.[24,25] The further use of these simulators to disentangle the wide range of processes that occur in the marine environment is being advanced by improvements in their construction and understanding the factors which are relevant for ideal operation.

While many ocean-atmosphere studies have focused solely on the composition and properties of freshly emitted nascent SSA (nSSA), atmospheric aging processes can transform SSA through reactions with trace gases, oxidants, and sunlight. For example, heterogenous reactions of SSA with HNO_3 results in the displacement of HCl, forming $NaNO_3$.[25] In addition, HNO_3 reacts with the basic sites present within biologically-derived organic molecules, such as lipopolysaccharides.[26,27] In addition to SSA, the oceans are a source of secondary marine aerosol (SMA), which is formed from the reactions of VOCs emitted from seawater. SMA can either form as new particles *via* nucleation or it can condense onto existing particles in the marine atmosphere, such as SSA, changing their size and chemical composition.[7] However, in field studies, it is extremely difficult to constrain the biological and chemical processes which lead to SMA formation and control its properties. Recently, oxidation flow reactors (OFRs) have been used to simulate both the heterogeneous oxidation of SSA and the formation of SMA in laboratory studies of marine mesocosms.[28–30]

Here we detail the features and usage of a newly constructed wave channel located at the Scripps Institution of Oceanography, focusing on performance and results from a two-month experimental campaign which focused on the production and measurement of marine aerosols. The Sea Spray Chemistry and Particle Evolution (SeaSCAPE) experiment was designed to study marine chemistry, microbiology, VOCs, and aerosols across the ocean-atmosphere interface, under clean, isolated conditions. To enable this, the wave channel was modified to optimize the production and collection of SSA. In contrast to previous wave channel experiments,[8,20] the SeaSCAPE experiment sought to probe the influence of atmospheric aging on the composition of marine aerosols. To this end, an ancillary sampling device was constructed to facilitate the study of marine gases and secondary aerosol formation from the seawater in the wave channel with minimal background contamination. Characterization experiments informed various modifications to wave channel construction and insights into best practices for operation, while also giving context for future analyses of data collected using this platform. We further outline the scope and scale of the SeaSCAPE

experiment, including selected results that demonstrate the types of new discoveries enabled by the mesocosm experiments discussed herein, with an emphasis on the incorporation of atmospheric oxidation processes.

2. Methods and materials

2.1 Description of wave channel

The Scripps Institution of Oceanography (SIO) wave channel is a 33 m × 0.5 m × 0.8 m ($L \times W \times H$) channel located inside the Hydraulics Laboratory. The wave channel is constructed of a series of 2 m long glass panels supported by a steel scaffold. When filled to a depth of 0.56 m with seawater, it holds a total water volume of 11 800 L (Fig. 1). Waves are generated by a paddle with a surface area of 0.96 m^2, powered by an electromagnetically driven linear motor (H2W Technologies). This design has key advantages over previously used hydraulically driven motors, mainly oil-free bearings and extended operation time. The paddle was operated at 0.3 Hz with a stroke length of 73 cm, which generates waves that break just beyond a submerged fiberglass ramp which functions as an artificial "beach" located midway down the channel (Fig. 1, Location 5). This beach (2.4 m in length) starts from the bottom of the flume channel and is positioned at an angle of approximately 16° relative to the bottom of the channel and sits ~5 cm below the quiescent water surface. Each breaking wave generates a plume of entrained bubbles with a similar size distribution and residence time as those in the ocean.[8,20] A second beach, located at the downstream end of the channel (Fig. 1, Location 10), serves to dissipate residual wave energy and prevent disruption of wave breaking at the primary beach. The top of the channel is sealed from the paddle tank to a distance 20.6 m downstream with acrylic lids, backed by marine-grade plywood for support (Fig. 1c). Adhesive backed foam strips were used to create a seal between the lids and the top of the wave channel, and then secured with vinyl-backed fabric tape. A PTFE sheet was suspended vertically from the last lid section to the water surface to reduce backflow of room air into the channel (Fig. 1, Location 7). In addition, the open section at the end of the wave channel was covered with lightweight polyethylene film to prevent dust and debris from settling into the channel.

Sampling ports for aerosol and gas measurements of the channel headspace were positioned at three locations throughout the wave channel (Fig. 1, Locations 4, 6a, 6b). The sampling ports consist of a stainless-steel bulkhead with a steel sampling tube which extend 0–10 cm below the lids into the headspace. An

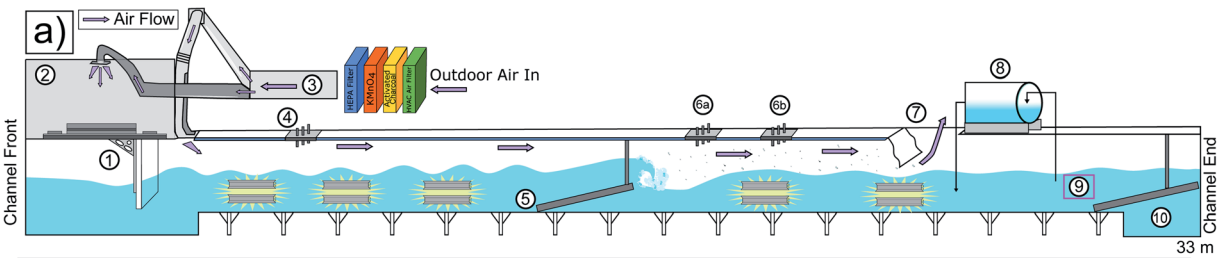

Wave Channel Location	Distance from Front (m)
① Reciprocating Paddle System	0-2.6
② PTFE Pressure Compensation Tent	0-2.6
③ Air Handling Entrance Ports	0,3.2
④ Upstream Sampling Port	6
⑤ Wave-Breaking Beach	10.9-13.3
⑥ Headspace Sampling Ports	16, 17.5
⑦ Headspace outlet, PTFE Isolation Film	20.6
⑧ Isolated Sampling Vessel	21.6
⑨ Bulk Water Sampling Location	28
⑩ Wave-Dampening Beach	29-33

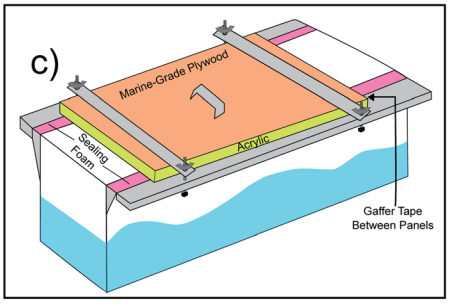

Fig. 1 (a) Schematic of the SIO Ocean-Atmosphere Interaction Facility (OAIF) wave channel with key points labeled by number and described in the table, (b) photograph of the SIO OAIF channel with key points marked, (c) cross sectional view of wave channel lids which were used to seal the channel headspace.

upstream sampling port located before the wave break was used to monitor background particle and gas concentrations (Fig. 1, Location 4). The sampling ports downstream from the wave break were used for measurements of SSA and VOCs (Fig. 1, Locations 6a, 6b). The two sampling locations were located 1.5 m apart to accommodate the large number of sampling devices, which were positioned on top of the wave channel.

The paddle assembly, including motors, is enclosed within a tent made of flexible PTFE film (TEKFILM, FEP2000E, 0.127 mm in thickness) to seal the system and prevent contamination from the room air, while accommodating pressure fluctuations caused by the reciprocating paddle. The box-shaped tent, which measures 244 cm length × 117 cm height × 80 cm depth, was fabricated with double heat-sealed edges and suspended in a stainless-steel frame over the paddle (Fig. 1, Location 2). The seam between the tent and the wave channel metal body was sealed using polyester tape (3M 8403, 5 cm diameter). Particle-free air was delivered to the wave channel from the top of the tent (Fig. 1, Location 3) using a custom air handling system made with galvanized steel duct pipes and stainless-steel connectors to the PTFE tent and the channel. Ambient air pulled in using a custom fan-blade powered by an induction motor (Marathon Electric 5THW8) was filtered through a four-stage filter system (Hydrosil International), consisting of a pre-filter, activated charcoal pellets, potassium permanganate ($KMnO_4$), and a HEPA filter. The scrubbed air was then directed into the wave channel headspace. The charcoal pellets served to reduce background VOC concentrations and the potassium permanganate served to remove acidic gases and other air pollutants. A condensation particle counter (CPC) positioned upstream of the wave break (Fig. 1, Location 4) was used to continuously monitor background particle counts in the headspace, indicating breakthrough from the filter system as well as leaks in the paddle tent. Headspace concentrations of NO_x, SO_2, and O_3, as well as air velocity, temperature, and relative humidity were also semi-continuously monitored from the same upstream sampling location (see Section 2.5.1).

The wave channel was equipped with fluorescent lights to provide the light flux necessary for photosynthetic organisms to grow within the seawater. Four light fixtures, two on either side, were attached to the outside of each 2 m glass panel of the channel below the water surface. Each fixture was equipped with two 120 cm fluorescent bulbs (Spectra 5700K F32-T8, Full Spectrum Solutions, Inc.), giving a total of 8 bulbs per panel. The lights extended the full length of the channel, except for the paddle tank at the front of the channel and the end tank, which are constructed of stainless steel and thus not transparent to light. The flux of photosynthetically active radiation (PAR) in the channel was measured to be ~80 μE m^{-2} s^{-1} in the center of the channel, approximately ~30 cm below the water surface (Apogee Instruments, MQ-200). While this is significantly lower than typical daytime PAR levels, which often exceed 1000 μE m^{-2} s^{-1} on clear days,[31] it is comparable to PAR levels reported in other studies for the purpose of growing marine phytoplankton.[32] To approximate day/night light cycles, the lights were operated on a timer which turned on for 14 hours during the daytime and off for 10 hours at nighttime.

2.2 Wave channel characterization experiments

Control experiments for characterizing the wave channel can be divided into two main types: (1) obtaining minimum background aerosol levels and (2) optimizing the sampling location and depth into the channel headspace. For the control experiments, the wave channel was filled with sand-filtered coastal seawater. This seawater is continually pumped from Ellen Browning Scripps Memorial Pier (Scripps Pier, 32-52′00″ N, 117-15′21″ W), filtered, and circulated directly into the research buildings at SIO, including the wave channel. As sand-filtration removes most of the large biological species (>1–2 μm) and results in microbiology that differs significantly from the seawater used in mesocosm experiments, this seawater was only used for wave channel characterization and testing.

2.2.1 Background particle concentrations. Total particle counts in the wave channel were measured before and after the wave break with condensation particle counters (Magic CPC, Aerosol Devices Inc.). The purpose of the upstream CPC was to detect ambient particle leaks in the paddle tent and the air handling system described in Section 2.1. Counts were typically very low (~3 #/cm^3). The downstream CPC measured the total number of particles after the breaking waves. Thus, we assume that the difference between upstream and downstream particle counts is the total number concentration of SSA generated by the breaking wave. During most of the study, the upstream counts were negligible, thus during these periods, we assumed that all the particles measured downstream were SSA generated by wave breaking.

2.2.2 Sampling location optimization. Aerosol size distributions of nSSA were measured using an Aerodynamic Particle Sizer (APS 3321, TSI Inc.) and a Scanning Mobility Particle Sizer (SMPS 3938, TSI Inc.) equipped with an X-ray neutralizer (Model 3088, TSI Inc.) at various locations downwind of the wave break (5 locations, 60 cm intervals) at 0–10 cm below the channel lid. The induction motor was tuned between 1250 and 2500 rotations per minute (RPM) to vary the airflow and determine the response of the total particle number concentration. Particles were dried prior to measurement with a silica diffusion dryer. The electrical mobility diameters (d_m) measured by the SMPS are assumed to be the same as the physical diameter (d_p). The aerodynamic diameters (d_a) measured by the APS were converted to physical diameter using the effective density of sea spray aerosol ($\rho_{eff} = 1.8$ g cm^{-3}).[9]

2.2.3 Wave channel headspace velocity. Measurements of the wave channel air velocity were obtained during paddle operation by injecting 50 μL of 45 mM dimethyl sulfide (DMS) in methanol into the wave channel headspace at the upstream sampling port. As DMS was carried along the length of the wave channel by the headspace flow, a home-built chemical ionization time of flight mass spectrometer (CI-ToF-MS) drew headspace at 2 slpm from the first downstream sampling port (Fig. 1, Location 6a). The operation of the CI-ToF-MS instrument is described in detail below (Section 2.6.2).

2.3 SeaSCAPE bloom initiation

2.3.1 Wave channel cleaning procedures. The wave channel was cleaned and sanitized prior to all experiments and induced bloom measurements. The channel was first filled and flushed with fresh water to remove any large debris, then the inside walls were sprayed with a 3% acetic acid/water mixture. A combination of soft sponges and brushes were used to manually remove any film or debris from the inner walls. Once completed, the channel was flushed with fresh water to remove all of the cleaning solution. As a final rinse, the channel was filled with sand-filtered seawater, then drained.

2.3.2 Water collection. Seawater was collected from the Scripps Pier. The water is pumped up from the end of the pier and travels through a gravity flume on the south side of the pier to the pier entrance. During the pumping process, the seawater passed through a rough aluminum screen to collect large marine detritus such as seaweed. A submersible pump (Grundfos UNILIFT AP12.40.04.A1) was placed into the gravity flume, and water was pumped through a hose into 1135 L plastic tanks and transported to the wave channel by truck immediately after filling at the Scripps Pier. The seawater was further filtered to remove large particulates and zooplankton using an acid-cleaned 50 μm Nitex nylon mesh (Flystuff; Cat # 57-106) and pumped into the wave channel. During Blooms 1 and 2, the Nitex mesh was attached directly to the outlet submersible pump, which inadvertently created shear forces which damaged some of the more delicate microorganisms in the seawater. To improve the seawater collection procedure, a gravity filtration system was used during Bloom 3. Briefly, a stainless-steel frame was built to fit over the top of the wave channel, to which a sheet of Nitex mesh with a surface area of $\sim$0.5 m^2 was affixed. Seawater was poured over the frame, allowing it to gently filter through the mesh.

2.3.3 Bloom initiation. Algae growth media and sodium metasilicate were added to the seawater at the beginning of each bloom cycle to promote phytoplankton growth.[33] The dates and concentrations of the nutrient additions are summarized in Table 1. The growth media was added at two locations: the upstream sampling ports (Fig. 1, Location 4) and after the end of the lid sections (Fig. 1, Location 9). Both the growth media and silicates were dissolved into several liters of milliQ H_2O, then slowly added dropwise to the channel using a sterilized separatory funnel or polycarbonate carboy equipped with a spigot over the course of several hours. This slow nutrient addition allows the growth media to mix with the seawater in the channel and prevents compounds from precipitating out of solution due to the high salinity.

During the third bloom cycle, a separate phytoplankton bloom was grown in a 1135 L cylindrical plastic tank outside of the hydraulics laboratory (Table 1). The purpose of this was to inoculate the wave channel with healthy phytoplankton biomass grown under natural sunlight to promote a larger bloom. Seawater was collected from Scripps Pier and filtered using 50 μm Nitex mesh, then it was transferred to the 1135 L outdoor tank, covered with wire mesh to keep out debris, and placed in partial shade. To stimulate the growth of a phytoplankton bloom, f/2 growth media and sodium metasilicate were added immediately and the seawater was bubbled gently to oxygenate. Once the outdoor tank reached the exponential growth phase as indicated by *in situ* fluorescence measurements (AquaFluor, Turner Designs), 1135 L of water were drained from the wave channel, and the contents of the tank were added to the wave channel. Water was transferred gently using sanitized buckets to avoid damaging the phytoplankton during the transfer. Additional nutrients were added to the wave channel immediately following the outdoor tank addition to bring the total concentration of growth media and silicates up to f/2 in the wave channel.

2.4 Isolated sampling vessel and OFR experiments

2.4.1 Description of isolated sampling vessel. Due to challenges associated with removing all trace gases from both the ambient air brought in *via* the air handler and off-gassing from wave channel materials, an isolated headspace was used to sample VOCs produced from seawater (see Section 2.6). The isolated sampling vessel (ISV) was constructed from a single cylindrical tube of borosilicate glass (Greatglas, Delaware U.S.A.) that was capped on both ends. The dimensions of the glass tube were as follows: 400 mm outer diameter, 6 mm wall thickness, 74 cm long, resulting in a total volume of 87 L and a water volume of 44 L, when filled halfway with seawater. An annotated schematic of the ISV can be found in Fig. S1.† Each end of the ISV was sealed by a PTFE disk, thickness 1.6 mm, braced against the face of the cylinder by a 9.5 mm acrylic disk and backed by an aluminum frame. Six 6.4 mm stainless steel Swagelok bulkhead ports in the headspace partition were used for the zero air inlet and gas sampling outlets (located on opposite ends), with one 13 mm bulkhead to continuously pump seawater and a 25 mm bulkhead drain port located 13 mm above the center of a PTFE sealing plate opposite of the filling bulkhead.

Table 1 Summary of seawater collection and nutrient additions during the three SeaSCAPE bloom cycles

Bloom cycle	Water fill date	Nutrient addition date	Nutrient concentration
Bloom 1	7/1/2019	7/4/2019	f/2 nutrients + silicates
Bloom 2	7/12/2019	7/14/2019	f/20 nutrients + silicates
Bloom 3	7/23/2019	7/25/2019	f/20 nutrients + f/40 silicates
		7/26/2019	Addition silicates, to f/20 total
		8/1/2019	Additional nutrients and silicates, to total concentration of f/2 for both

Seawater was delivered to the ISV *via* a plunging stream located opposite the sampling ports. The seawater was circulated using a peristaltic pump equipped with Tygon tubing, which withdrew water from the wave channel, ~0.5 m beneath the water surface. In order to maintain a consistent flow rates and prevent leaks, the tubing within the peristaltic pump was replaced every 3 days. ISV water drained back into the channel through 25 mm tubing attached to the large central port opposite the plunging jet, with the end of the return flow tubing submerged beneath the water level. Zero air flow rate through ISV headspace varied from 8–10 standard liters per minute (slpm), leading to an average air residence time of 5 minutes. The water flow rate was fixed at 1.5 slpm, leading to a water residence time of 29 minutes. The ISV was lit by two fluorescent light fixtures, which extended the length of the vessel on either side. These lights were identical to those used on the wave channel and were operated on the same diurnal pattern, for the purpose of maintaining the same light flux in the ISV during daytime hours.

2.4.2 OFR operation. To study the effect of atmospheric aging processes on marine aerosols, potential aerosol mass oxidation flow reactors (PAM-OFR, Aerodyne Inc.) were used to simulate both the heterogeneous oxidation of primary sea spray aerosol and the formation of secondary marine aerosol from the oxidation of VOCs. The PAM-OFR uses UV lamps to produce high concentrations of OH radical, simulating atmospheric aging from a fraction of a day to weeks, with a residence time of 1–3 minutes.[34,35] Two OFRs (OFR1 and OFR2) sampled from the wave channel headspace (Fig. 1, Location 6a), with the goal of producing heterogeneously aged SSA (hetSSA), although SMA is also produced from the oxidation of VOCs present in the wave channel headspace. Fig. S2† shows a schematic of the different OFR sampling lines utilized during SeaSCAPE. Briefly, OFR1 was utilized for continuous, online measurements of hetSSA chemical composition, size distributions, and hygroscopicity. In contrast, OFR2 was utilized for a combination of online and offline measurements including aerosol chemical composition, phase and morphology, and INP characteristics. A third OFR (OFR3) sampled from the ISV (Fig. 1, Location 8), for the purpose of producing SMA under clean conditions. A full inventory of aerosol measurements conducted using the OFRs can be found in Tables 2 and 3.

All OFRs were operated in OFR185 mode, meaning the UV lamps produce light with wavelengths of both 185 nm and 254 nm. The OH exposure at each lamp intensity was determined by introducing carbon monoxide to the OFR and measuring the drop in CO concentration due to oxidation using a CO analyzer (APMA-370, Horiba Ltd). The OH exposure is determined using the rate coefficient of CO + OH ($k_{OH+CO,\ 298K} = 1.5 \times 10^{-13}$ cm^3 molec^{-1} s^{-1}), assuming pseudo-first order

Table 2 Summary of all online aerosol measurement techniques employed during SeaSCAPE. The sample type is designated by a single letter (N = nascent SSA, H = heterogeneously-aged SSA, S = secondary marine aerosol)

Measurement	Technique	Sample type	Sampling interval	Ref.
Dry particle size distributions from 5 nm to 20 μm	Scanning Mobility Particle Sizer (SMPS, TSI Inc.)	N, H, S	2–5 min	85
	Aerodynamic Particle Sizer (APS 3321, TSI Inc.)	N, H	1 min	86
	Scanning Electrical Mobility Spectrometer (SEMS, Brechtel)	N, H	5 min	87
Total particle number	Condensation Particle Counter (CPC)	N	1 s	88
Single particle composition and size	Aerosol Time-of-Flight Mass Spectrometer (ATOFMS)	N, H	1 min	89
Size-resolved non-refractory submicron aerosol composition	High Resolution Time-of-Flight Aerosol Mass Spectrometer (HR-ToF-AMS)	N, H, S	5 min	40
Ultrafine aerosol chemical composition	Thermal Desorption Chemical Ionization Mass Spectrometer (TDCIMS)	N, S	N: 1 h, S: 30 min	90 and 91
Submicron aerosol chemical composition	Extractive Electrospray Ionization Mass Spectrometry (EESI-MS)	N, H, S	1 s	92
Size-resolved cloud condensation nuclei activity	Continuous-flow streamwise thermal-gradient CCN counter	N, H, S	30–60 min	93
Relative humidity-dependent aerosol bounce	Electrical Low Pressure Impactor (ELPI)	N, H, S	1 min	94
INP concentration	Continuous-Flow Diffusion Chamber (CFDC)	N, H	5–15 min	95
Size-resolved fluorescent biological particle number concentrations	Wideband Integrated Bioaerosol Sensor (WIBS)	N, H	1 s	96

Table 3 Summary of all offline aerosol measurement techniques employed during SeaSCAPE. The sample type is designated by a single letter (N = nascent SSA, H = heterogeneously-aged SSA, S = secondary marine aerosol)

Measurement	Collection technique	Analysis technique	Sample type	Sampling interval	Ref.
INP concentration and characteristics	Polycarbonate filters	Ice spectrometer	N, H	1–5.5 h	97
Size-segregated organic aerosol composition	Sioutas cascade impactor	High resolution mass spectrometry	N, H	6–12 h	98 and 99
Single particle morphology, phase state, organic volume fraction, and water uptake	MOUDI impactor	Atomic Force Microscopy (AFM)	N, H	N: 5–6 h, H: 1–2 h	39 and 100
		AFM photothermal infrared spectroscopy (AFM-PTIR)	N, H	N: 5–6 h, H: 1–2 h	101
Immersion freezing of single particles	MOUDI impactor	Micro-Raman spectroscopy	N, H	1–2h	102
Aerosol pH	MOUDI impactor	pH paper	N	1–2 h	103
Chemical and microbial composition	Quarts fiber filters	High-resolution mass spectrometry	N	24 h	104
		16S/18S rDNA sequencing	N	24 h	19
Viral and bacterial abundances	Spot sampler	Flow cytometry	N	4–6h	54 and 55
Enzymes activities	Spot sampler	Fluorogenic substrates	N	6 h	59 and 105
Submicron aerosol speciated organic chemical composition	Quartz fiber filters	TD-GCxGC-EI-HRToF-MS	N	14 h/10 h (day/night)	49
Submicron and supermicron isotopic analysis	Cyclone and quartz fiber filters	MAT 253 isotope-ratio mass spectrometry (IRMS)	N	48 h	106

kinetics.[36] The OH exposure can be converted to "days of equivalent aging" using typical tropospheric OH concentrations ([OH] = 1.0×10^6 molec cm^{-3}).[37] O_3 concentrations were monitored downstream of each of the OFRs using an O_3 analyzer (Model 202 and Model 106-L, 2B Technologies). Before aerosol measurements, the sample air was passed through a denuder to remove O_3 (Carulite-200, obtained from Ozone Solutions).

2.5 SeaSCAPE – aerosol measurements

A large suite of aerosol measurements was conducted during the SeaSCAPE experiment to study the properties of nSSA, hetSSA, and SMA. These include measurements of the size distributions, chemical composition, INP characteristics, CCN activity and water uptake, and phase state and morphology, among other properties. All measurements conducted during the campaign are summarized in Tables 2 and 3.

2.5.1 Aerosol number and size distributions. Total particle counts in the wave channel were measured before and after the wave break with condensation particle counters. The aerosol size distributions of nSSA after the wave break were measured using the APS and SMPS as described in the control experiment. Size distributions from OFR1 and OFR2, which includes both hetSSA and SMA, were measured using a Scanning Electrical Mobility Spectrometer (SEMS, Brechtel Manufacturing, Inc.) and an APS (3321, TSI Inc.). SMA size distributions from OFR3 were measured using an SMPS (Model 3938, TSI Inc.) equipped with a Nano DMA (DMA 3085, TSI Inc.) and a soft X-ray Neutralizer (Model 3088, TSI Inc.). The SMPS and APS systems were factory calibrated prior to the SeaSCAPE campaign. During the study, polystyrene latex spheres (PSLs) were used to verify the sizing instrument performance.

2.5.2 Single particle Atomic Force Microscopy (AFM) measurements. Nascent and heterogeneously aged sea spray aerosols were collected for AFM measurements of aerosol phase and morphology throughout SeaSCAPE. A selected analysis was conducted of particles collected on 8/3/19, which corresponded to the peak of the phytoplankton growth during Bloom 3. The nSSA were deposited onto hydrophobically treated silicon substrates (Ted Pella, Inc.) using a micro-orifice uniform deposit impactor (MOUDI, MSP, Inc., model 110, flow rate of 30 lpm) at *ca.* 80% RH (*i.e.* wet deposition).[38] The hetSSA were deposited onto the hydrophobically treated silicon substrates using a separate MOUDI (MSP, Inc., model 125R, flow rate of 10 lpm) at *ca.* 20% RH (*i.e.* dry deposition).[38,39] MOUDI stages 6, 7 and 8 were used, which corresponds to an aerosol aerodynamic diameter 50% cut off range of 0.18–1.0 μm. The hetSSA were generated using OFR2, with a UV lamp voltage of 2.0 V which corresponds to approximately 4–5 days of photochemical aging in the atmosphere. The substrate-deposited nascent and hetSSA samples were stored in clean Petri dishes and kept inside a laminar flow hood (NuAire, Inc., NU-425-400) at ambient temperature (20–25 °C) and pressure.

AFM height images of individual nascent and hetSSA particles were recorded using the molecular force probe 3D AFM (Asylum Research, Santa Barbara, CA), at ambient temperature (20–25 °C) and pressure. Silicon nitride AFM tips (MikroMasch, Model NSC35, tip radius of curvature ~10 nm) were used to image individual particles. A custom-made humidity cell was used to control the RH at 50% for all imaging; the elevated RH was used due to expected lowering of the viscosity for the organic components relative to inorganic that facilitates differentiation of their spatial distribution using AFM.[38] AC mode (intermittent contact or tapping mode) AFM was used to image individual particles and determine their morphology. A

total of 50 individual particles were characterized for each sample type.

2.5.3 Aerosol Mass Spectrometry (AMS). The chemical composition of submicron non-refractory aerosol was determined by high resolution time-of-flight aerosol mass spectrometry (HR-TOF-AMS; Aerodyne, Inc.).[40] A collection efficiency of CE = 0.65 was applied to the data. The AMS was operated in V-mode with standard MS mode (5 s open, 5 s closed) and PTOF (10 s) with typically 5 min sampling averages.

2.6 SeaSCAPE – gas-phase measurements

In addition to the gas-phase measurements discussed below, Table 4 details the full inventory of gas-phase measurements conducted during SeaSCAPE to assess questions regarding VOCs produced from seawater and anthropogenic contaminants.

2.6.1 Trace inorganic gases. The concentrations of trace gases were monitored at several locations: the air handling system, room air, and the wave channel headspace, upstream of the wave break. A custom-fabricated solenoid valve switching array was used to automatically switch between the different air sampling lines. The concentrations of the oxides of nitrogen (NO_x) were continuously monitored using a Model 42C NO–NO_2–NO_x analyzer (Thermo Electron Corporation). Ozone concentrations were measured using a UV photometric based O_3 analyzer (Model 49C, Thermo Electron Corporation). The analyzer was calibrated using an ozone calibration source (Model 306, 2B Technologies). Sulfur dioxide concentrations were measured using a pulsed fluorescence SO_2 analyzer (Model 43iQ Trace Level SO_2 Analyzer, Thermo Electron Corporation).

2.6.2 Chemical ionization time of flight mass spectrometry. A home-built CI-ToF-MS using benzene cluster cation chemistry, previously described by others,[41,42] was utilized to determine the headspace flow rate of the wave channel. Briefly, ~300 ppm benzene vapor was generated by passing 10 standard cubic centimeters per second (sccm) of N_2 over a cylinder of liquid benzene and diluted to concentration with added N_2.[42,43] Benzene vapor was passed through a 20 mCi Po-210 α-source to generate benzene cluster cation reagent ions, and further drawn through an inline critical orifice at 1.8 slpm into the ion-molecule region (IMR) of the CI-ToF-MS. Sample analyte was similarly drawn into the IMR at the same flow rate as analyte. The IMR pressure was maintained at 60 torr and 60 V for all analyses. Analyte ions generated through charge transfer and ligand switching reactions with benzene cluster cations were focused by a radio frequency ion funnel, and subsequently transferred by an RF-only quadrupole into an orthogonal-extraction time of flight analyzer (Tofwerk). Co-summed mass spectra from 5–500 m/z were obtained at 1 Hz, with generated data analyzed using the Tofware plugin for Igor Pro 7 software.

2.6.3 Proton transfer reaction mass spectrometry. A Vocus proton transfer reaction time-of-flight mass spectrometer (PTR-ToF-MS) (TOFWERK, Aerodyne Inc.) measured headspace gas-phase VOCs.[44] The focusing ion-molecule reactor was operated at high reduced field strength (E/N = 143 Td). It was held at a pressure of 1.5 mbar, electric field of 41.5 V cm^{-1}, and temperature of 100 °C. The big segmented quadrupole voltage was 275 V, reducing the transmission of low mass (<35 m/Q) ions. The PTR-ToF-MS mass spectra were saved at 1 Hz time resolution. The headspace of the ISV was sampled at 100 sccm through a roughly 2.5 m, 6.35 mm O.D. PFA tube. The air handling system and wave channel headspace were pulled down a 9.525 mm O.D. PFA tube approximately ~15 m at a flow rate of 8 slpm. The PTR-ToF-MS subsampled 100 sccm of this flow. Room air was sampled intermittently approximately 8 times throughout the day. Instrument background signals were determined about 8 times daily by overflowing the PTR-ToF-MS inlet with zero air from the zero-air generator (Sabio 1001) that provided air to the ISV headspace. Daily average background signals were used for background correction. Peak fitting and integration were completed in Tofware 3.1.2.

2.6.4 Offline atmospheric pressure chemical ionization for irradiation experiments. Photo-initiated VOC production was measured using a high-resolution Orbitrap Elite (Thermo Fisher Scientific) mass spectrometer equipped with a modified gas-phase atmospheric pressure chemical ionization (APCI) source. Seawater samples collected during the SeaSCAPE campaign were irradiated using an LCS-100 solar simulator

Table 4 Summary of all gas-phase measurement techniques employed during SeaSCAPE. The sample type is designated by a single letter (W = wave channel headspace, I = isolated sampling vessel headspace, D = dissolved gases, A = air handling system, O = OFR, B = bulk seawater, L = SSML)

Measurement	Technique	Sample type	Sampling interval	Ref.
O_3	UV absorption, Thermo Environmental Model 49C	W, A	1 s	N/A
	UV absorption, 2B Technologies Model 202	O	1 s	N/A
NO–NO_2–NO_x	Chemiluminescence, Thermo Environmental Model 42C	W, A	1 s	N/A
SO_2	Pulsed fluorescence, Thermo Environmental Model 43iQ	W, A	1 s	N/A
VOCs	Vocus Proton Transfer Reaction Mass Spectrometry (PTR-ToF-MS)	W, I, A	1 s	44
Sulfur-containing VOCs	Chemical Ionization Mass Spectrometry (benzene reagent ion, B-CI-ToF-MS)	I, D	1 s	42
Speciated VOC's (isomer specific)	TD-GCxGC-EI-HRToF-MS	I	20 min collection, every 1–3 days	46
Abiotic photo-enhanced surface products	Gas phase modified-atmospheric pressure chemical ionization Orbitrap mass spectrometry (APCI-MS)	B, L	24 h	45

(94011A, Oriel), adapted from the approach used by Roveretto *et al.*[45] Data were collected solely in positive mode, where needle voltage was set to 4 kV, needle current at 5 mA, and vaporizer temperature at 150 °C. Sheath and auxiliary flow were set to zero. An air mass optical filter (AM 1.5G, Newport Inc.) and a water filter were used to simulate the solar spectrum and block infrared radiation, respectively. From the wave channel, 200 mL of surface water was collected and transferred into a 350 mL jacketed custom glass tube (Ace Glass Inc.) with a quartz window on each end. The surface area of the water sample in the tube was approximately 77 cm^2. With a headspace of 150 mL, pure nitrogen gas was used as a carrier at a rate of 200 sccm. Temperature was regulated and measured constantly to ensure minimal thermal variation (±1 °C) during the experiment. The collected water settled for 2 hours before being irradiated to allow a stable surface layer to form. To verify whether the immediate spike in signal was abiotic or biotic in nature when under lighted conditions, a separate experiment using the same water, but filtered with a 0.2 μm GTTP filter (MilliporeSigma) to remove most biological material.

2.6.5 Thermal desorption two-dimensional gas chromatography. VOCs from the ISV and from the offline irradiation experiments were collected on triple bed sorbent tubes (Tenax TA, Carbograph 1, Carboxen 1003, CAMSCO). Samples were collected at 100 sccm for 20 minutes from the ISV headspace and 200 sccm for 10 minutes from the offline irradiation experimental setup. Samples were frozen immediately after collection and were analyzed offline by Thermal Desorption (Gerstel TD 3.5) two-dimensional Gas Chromatography (Agilent 7980 A), modulated by two stage thermal modulation (Zoex), coupled with variable energy Electron Ionization Time of Flight Mass Spectrometry (Markes BenchToF) (TD-GCxGC-EI-ToF-MS). Data was collected at 50 Hz, and ionization energies oscillated rapidly between 70 eV and 14 eV to simultaneously generate two sets of chromatograms for each sample. The hard ionization (70 eV EI) significantly fragments analytes to produce structure-specific fragmentation patterns, whereas the soft ionization (14 eV EI) preserves the parent ion for comparison to chemical ionization techniques. Column materials and thermal methods are as described in Hatch *et al.*[46]

2.7 SeaSCAPE – water measurements

Seawater measurements sought to characterize both the biotic and abiotic drivers of marine particles and gases, including nutrient availability, organic chemical composition, biological speciation, biological productivity, dissolved gas turnover and

Table 5 Summary of all seawater and SSML measurements collected during SeaSCAPE. The sample type is designated by a single letter (L = SSML, B = bulk seawater)

Measurement	Technique	Sample type	Sampling interval	Ref.
Chlorophyll-a	Continuous fluorescence (ESP)	B	1 min	20
	Fluorescence (AquaFluor)	B	24 h	20
	Extracted fluorescence	B	24 h	50
Dissolved O_2	Continuous optical absorption	B	1 min	107
Bacterial community composition	Amplicon sequencing	B, L	24 h	108
Heterotrophic bacteria concentration	Flow cytometry	B, L	24 h	54
Virus concentration		B, L	24 h	55
Nano-pico-phytoplankton and heterotrophic nanoflagellates concentration		B, L	24 h	56 and 109
Phytoplankton community	*In situ* camera	B	10 Hz	53
	Microscopy and sequencing	B, L	24 h	110
Dissolved organic carbon	High temperature catalytic combustion (Shimadzu TOC-V series instrument)	B	Daily	111
Speciated DOM organic compounds	HR-ESI-MS	B	72 h	80
	TD-GCxGC-EI-HRToF-MS	B, L	72 h	49
Nutrients (NO_3, NO_2, PO_4, SiO_4, NH_4)	Seal analytical continuous-flow AutoAnalyzer 3	B	24 h	112
Alkalinity, bicarbonate, carbonate, dissolved inorganic carbon, dissolved CO_2, salinity, pH	Combined pCO_2/TCO_2 Dual Analyzer	B	1 Hz	113
Water temperature	Thermocouple (ESP)	B	1 min	20
Enzyme activity	Fluorogenic substrates	B, L	24 h	105
Bacterial production/growth rate	3H-Leucine incorporation	B, L	24 h	114
Methylotrophy	C14-methanol incorporation	B, L	24 h	115
DMSPp, DMSPd, [DMS]aq	Cryo purge and trap benzene CI-ToF-MS	B	24 h	42 and 116
Functional genes and transcripts dddP, dmdA	Q-PCR for quantification, and sequencing	B, L	24 h	117
INP concentration and characteristics	Ice spectrometer	B, L	24 h	97
Fluorescent DOM	Fluorescence excitation emission matrix spectroscopy (EEMS)	B, L	24 h	80
HONO production from DOM	Incoherent broadband cavity-enhanced absorption spectroscopy (IBBCEAS)	B	End of Bloom 3 only	118

other important factors. Table 5 lists the seawater and sea surface microlayer (SSML) measurements made through the duration of SeaSCAPE.

2.7.1 Bulk seawater sampling. Bulk seawater was sampled daily from the end of the wave channel (Fig. 1, Location 9) for the following analyses: dissolved organic carbon (DOC); inorganic nutrients; extracted chl-a; bacterial and viral abundances; phytoplankton identification; enzyme measurements; 16S and 18S rDNA amplicon sequencing; and tandem mass spectrometry (MS/MS) based metabolomics. Seawater was collected using a ~2 m long siphon constructed from Teflon tubing. Nalgene carboys were used to transport and dispense the collected seawater for analysis. Both the siphon and the carboys were rinsed with methanol, 70% ethanol, 0.1 M HCl solution, and ultra-purified water prior to water collection. The siphon was inserted approximately 20 cm below the surface of the water. Approximately 16 L of bulk seawater were collected daily around 09:30 PST. The volume of collected seawater was replenished by adding a corresponding volume of Milli-Q (Millipore) water (<18 μΩ) every other day to maintain the water level in the flume without introducing any microbiological contaminants.

2.7.2 Sea surface microlayer sampling. Sea surface microlayer (SSML) samples were collected from the same location as the bulk seawater (Fig. 1, Location 9). The collection was conducted using a glass plate, a glass funnel and a Teflon scraper. During the day preceding collection of SSML samples, the glass plate and funnel were cleaned of biological material using Millipore water, methanol, 70% ethanol, and 10% HCl. The collection glassware was placed in a combustion furnace for 5 hours at 500 °C to remove organic contaminants. The glass plate with a handle was lowered carefully into the wave channel at a rate of 5–6 cm s^{-1} and withdrawn at the same rate. This withdrawal rate corresponds to an estimated sampled SSML thickness of around 50 μm.[47,48] After removal from the wave channel, the glass plate was suspended for 20 seconds to allow any bulk seawater to drain off the plate and back into the channel, ensuring that the majority of remaining material was SSML. The remaining liquid was scraped from the glass plate into a collection vessel using a Teflon scraper. This process was repeated until approximately 200 mL of sample was collected.

2.7.3 DOM extraction and compositional analysis. Dissolved organic matter (DOM) was extracted from bulk seawater samples collected from the wave channel (Fig. 1, Location 9) using the solid phase extraction method described and characterized by Dittmar and coworkers (Dittmar 2008). At the end of Bloom 3, a large volume of about 2000 L was extracted over the course of 72 hours using this method. A total of 1.51 ± 0.01 g of marine DOM was collected and stored at −18 °C for future analyses.

Samples of extracted DOM were analyzed by TD-GCxGC-EI-HR-ToF-MS. DOM samples were reconstituted in methanol immediately prior to analysis and injected onto quartz fiber filter segments, then doped with a custom blend of 23 deuterated internal standard compounds prior to analysis, allowing corrections for instrument condition and matrix effects across samples. Briefly, the instrument thermally desorbs samples from the filter media, then introduces them into the GC oven. The instrument employs online derivatization during thermal desorption with MSTFA (*n*-methyl-*n*-trimethylsilyl-trifluoroacetamide). Analytes are separated by volatility and then by polarity by two GC columns in sequence. Separated analytes from are ionized by 70 eV electron ionization (EI) and detected by HR-ToF-MS (Tofwerk). Methodological details follow Worton *et al.*[49] Six-point calibration curves of custom standard blends containing ~150 representative organic compounds were performed periodically throughout sample analysis for each sample medium class to maximize quantification accuracy.

2.7.4 Chlorophyll-a, dissolved oxygen, and DOC measurements. A continuous time series of *in vivo* chl-a and dissolved oxygen was measured throughout all three wave channel experiments using an Environmental Sample Processor (ESP). The ESP was located at the back of the wave channel just before the wave-dampening beach (Fig. 1, Location 9). The ESP is a homemade, continuous flow system that pumps seawater through tubing at a flow rate of ~1 lpm using a peristaltic pump. The seawater first passed an SBE 37 MicroCAT that measures conductivity, followed by an SBE 63 optical dissolved oxygen sensor before being deposited into a reservoir. In the reservoir, chl-a is quantified through fluorescence measurements using a Sea Bird Scientific ECO-Triplet-BBFL2 sensor at excitation/emission wavelengths of 470/695 nm. After measurement of chl-a, the seawater is circulated out of the ESP and back into the wave channel.

Each morning, the ESP was rinsed by circulating Millipore water through the tubing for 20 minutes, and every fourth day, solutions of 0.1% bleach, 30% ethanol, and Millipore water were sequentially circulated through the tubing for 20 minutes to thoroughly clean the instrument. This helped prevent biological growth in the tubing and biofouling of the optics. Additionally, in between each experiment, the reservoir was removed from the laser optics and both were carefully wiped with 70% ethanol. Any ESP measurement periods that were affected by instrument maintenance or biofouling were corrected using *in vivo* chl-a measurements made by a hand-held fluorometer (AquaFluor, Turner Designs). AquaFluor chl-a measurements were made every few hours from the seawater sampling section of the wave channel.

To calibrate both the ESP and AquaFluor chl-a measurements, chl-a was extracted from the bulk seawater and analyzed by fluorometric analysis in accordance with CALCOFI methods.[50] The seawater was collected once daily from the wave channel (as described in Section 2.7.1) and filtered on 25 mm Whatman GF/F filters. The filters were then submerged in 8 mL of 90% acetone for 24 hours at −20 °C to extract the chl-a. Concentrations of the extracted chl-a were determined by a calibrated fluorometer (10 AU, Turner Designs). The extracted chl-a measurements were separately plotted against both the ESP and AquaFluor data, and each plot was fitted with a least squares regression used to calibrate the ESP and AquaFluor chl-a values. A continuous time series of the calibrated ESP chl-a data for all three experiments is shown in Fig. 2.

For DOC measurements, two 40 mL aliquots of the bulk seawater (see Section 2.7.1 for details of water collection) were

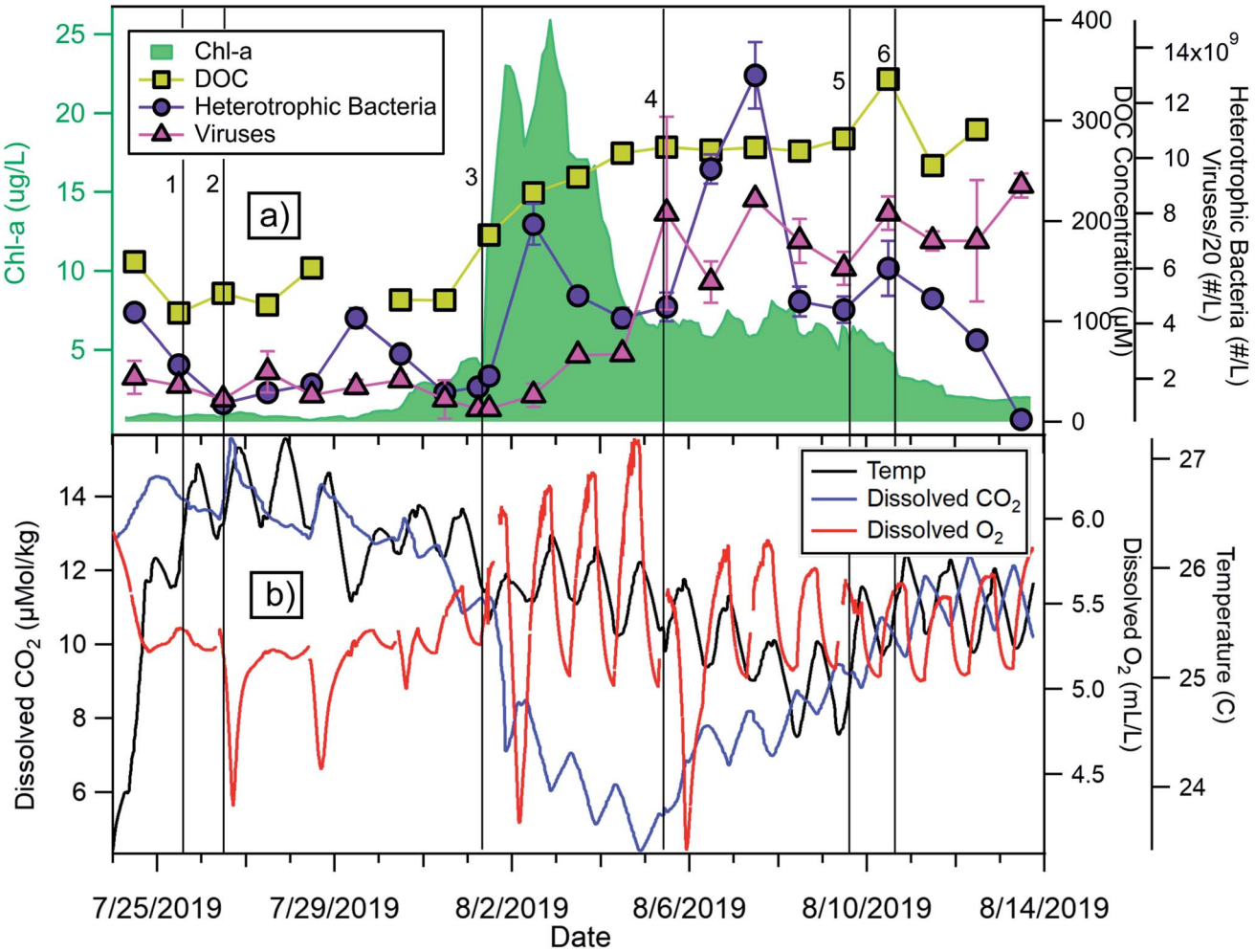

Fig. 2 (a) SeaSCAPE Bloom 3 chl-a, DOC, heterotrophic bacteria, and virus counts over the mesocosm duration. Numbered vertical lines indicate notable interventions in mesocosm. Lines 1 and 2 correspond to nutrient additions specified in Table 1. Line 3 corresponds to the addition to the wave channel of water from an outdoor tank in which a bloom was induced from the same source water. Line 4 corresponds to the scraping of wave channel walls to remove light-obstructive detritus. Lines 5 and 6 correspond to the addition of circulating pumps to resuspend cellular material that had settled on the wave channel bottom. (b) Bloom 3 water temperature, dissolved CO_2, and dissolved O_2.

filtered into combusted glass vials through a Whatman GF/F filter, which has a pore size of 0.7 μm.[51] Functionally this implies that the DOC was comprised of OC with diameters <0.7 μm. The vacuum filtration was carried out using a hand pump to minimize cell lysis during filtration. The DOC samples were immediately acidified to pH ~2 with three drops of concentrated HCl and stored in a covered box at room temperature until analysis. All DOC concentration measurements were made on a Shimadzu TOC-V_{CSH} catalytic combustion oxidation instrument.

2.7.5 Phytoplankton enumeration and photography. In order to determine the taxonomic composition of the mesocosm, two methods were employed: (1) whole seawater samples were collected and manually counted under confocal microscopy; (2) a dual version of the Scripps Plankton Camera System (SPCS: https://spc.ucsd.edu) was placed on the bottom of the wave channel to continuously image the developing plankton community for *in situ* observations. The SPCS was positioned at the downstream end of the channel, just in front of the dampening beach (Fig. 1, Location 9). For the manual counting method, 400 mL of seawater was collected from approximately 30 cm depth at both ends of the wave channel. Samples were taken twice per day with Teflon tubing and poured gently into amber Nalgene bottles. Samples were immediately fixed with a 2% buffered formalin solution and stored at 6 °C to preserve samples for enumeration. From these, 50 mL subsamples were then poured into a settlement chamber and allowed to settle for 24 h. The cells were prepared for enumeration using the Utermöhl method under an Olympus IX-71 inverted microscope.[52] Samples from the settlement chamber were counted to calculate the cell concentrations per L for each distinct species. Then, the taxa cell counts were binned into functional phytoplankton types, including a microzooplankton group. These bins were used to calculate the relative abundance of the functional groups over time and were then compared to the *in situ* camera data.

The *in situ* camera enabled the research team to study the plankton community undisturbed in the mesocosm, monitor the presence of delicate taxa, and observe intra- and inter-species interactions. The goal of the image analysis was to target detritus, aggregates, phytoplankton and zooplankton between 20–1000 μm in major axis length. For this reason, only images collected by the 5× magnification system of the SPCS were considered. Over the course of the 3 week experiment, nearly 1.85×10^6 images of particles were collected within this size range. The system uses darkfield illumination to image free-floating particles in approximately 3 μL per frame sampling volume with a resolution of 3–5 μm.[53] In order to train a neural net to classify this large amount of data, a subset of the images was manually labelled to serve as a training set.

2.7.6 Bacteria, virus, nano-and picophytoplankton, and heterotrophic nanoflagellates enumeration. Bacteria, cyanobacteria and viruses in the seawater, SSML and nSSA were enumerated with a BD FACSCanto II™ flow cytometer (FCM). Samples were prepared according to established protocols.[54–56] All samples were preserved with glutaraldehyde at 5% final concentration and stored at −80 °C.[57] For heterotrophic bacteria staining, the samples were diluted with Tris–EDTA buffer (pH 8), then stained with SYBR Green.[54] For virus staining, water was diluted (1 : 50) in 1× TE buffer (pH 8) and stained with SYBR Green.[55] Aliquots of seawater and SSML samples were analyzed unstained for counting *Cyanobacteria*.[58] SSA samples were collected into 0.7 mL 4× PGE (prepared as 4× PBS, 20% glycerol, 20 mM EDTA) buffer using a Liquid Spot Sampler (SS110A, Aerosol Devices Inc.), which sampled at 1.8 lpm.[59] The liquid sample was brought to 1 mL by adding 4× PGE, then split into two 0.5 mL aliquots that were processed as described above for FCM counting of heterotrophic bacteria and viruses. SSA blank samples were also collected *via* Spot Sampler with a HEPA filter on the inlet and processed accordingly. The values counted in the same SSA blank gates were subtracted from the SSA sample runs. For heterotrophic bacteria and viruses, the samples were analyzed at medium rate (60 μL min^{-1}) with a threshold set on green fluorescence. Side scatter *versus* green fluorescence plots were generated to identify and quantify heterotrophic bacteria and viral populations.[56,58] Synechococcus population were identified on forward scatter *versus* orange fluorescence and red fluorescence. Samples for nano, picophytoplankton and heterotrophic nanoflagellates were run on a BD Accuri FCM following established protocols.[60,61]

3. Results: characterization and optimization of the wave channel

3.1 Contaminant contributions to wave channel headspace composition

The concentration of trace inorganic gases (NO_x, SO_2, CO, and O_3) were monitored in the wave channel headspace, as the air handling system is not expected to fully remove these gases. In the remote marine boundary layer, NO_x mixing ratios are typically less than 50 ppt.[62] During the SeaSCAPE campaign, the

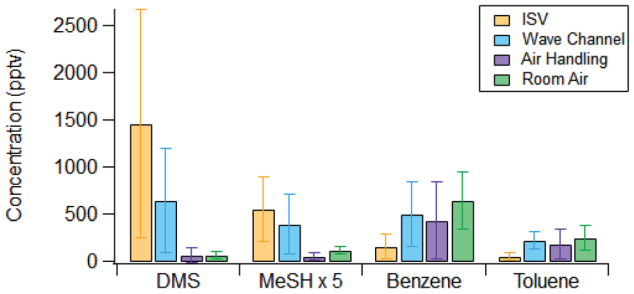

Fig. 3 Histogram comparing daytime mixing ratios of DMS, MeSH, benzene, and toluene in the isolated sampling vessel (ISV), wave channel headspace downstream of wave-breaking, air handling system, and hydraulics laboratory room air. Bars show the averages over the entirety of Bloom 3, and error bars represent the 1σ standard deviation over the daily average measurements.

NO_x concentration in the channel headspace was significantly higher, with a mean concentration of 1.4 ppb (Table S1 and Fig. S3†). This is lower than typical ambient concentration expected in an urban area (10–100 ppb),[63] indicating that the air handling system was able to scrub some ambient NO_x; however, it was not able to achieve levels as low as the clean marine boundary layer. Conversely, while the air handling system failed to remove all of the O_3 from the headspace air, the resulting concentrations (average $[O_3] = 16$ ppb, Table S1†) were actually comparable to background concentrations observed in the Atlantic boundary layer (~15–20 ppb).[64]

Volatile organic compounds were measured in the wave channel headspace, air handling system, ISV, and room air, with PTR-ToF-MS to determine whether they originate from a marine biogenic source or anthropogenic contamination (Fig. 3). Dimethyl sulfide (DMS) and methanethiol (MeSH) were chosen as proxies for expected marine biogenic VOCs in comparison to benzene and toluene which are more closely associated with anthropogenic pollutants and are not expected to be produced

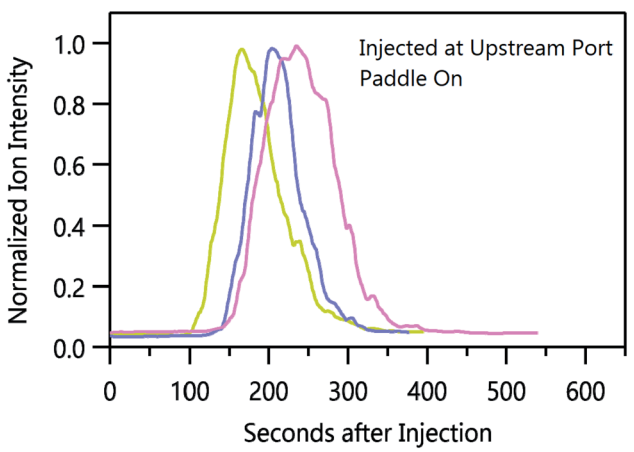

Fig. 4 Replicate experiments of dimethyl sulfide (*m*/*z* 62) arrival time at the downstream sampling port measured by CI-TOFMS. Instrument signal was boxcar smoothed into 10 second bins. Sample injections were made sequentially on the same day.

biogenically in large quantities in the marine environment.[65] Fig. 3 shows that benzene and toluene were most elevated in room air, the air handling system, and the wave channel headspace, but were significantly diminished in the ISV. These results suggest that the primary source of benzene and toluene in the wave channel was not derived from the seawater, but likely as breakthrough of the air handling system. Conversely, the concentrations of DMS and MeSH in the ISV were significantly elevated compared to the wave channel, due to the lower air flow rate and higher relative water surface area. These results show that the ISV was effective in maintaining a clean headspace that better reflects the emissions of gases present in seawater with minimal anthropogenic background.

3.2 Wave channel headspace velocity

Given the unique aspects of the wave channel, which features a highly longitudinal construction, with air introduction at one side, and a propagating water wave inside, a short investigation was undertaken to determine the headspace flow velocity along the channel length at a fan speed of 1500 RPM using spikes of injected DMS at the upstream port. Shown in Fig. 4 is the arrival of DMS spikes at the downstream sampling port (Fig. 1, Location 6a) measured by CI-ToF-MS. Mean arrival time was 200 $\pm$ 35 seconds ($N = 3$) with the paddle running. Replicate experiments with the paddle stationary did not yield arrival times that significantly differed. Given the distance of the upstream sampling port from the downstream ports, the wave channel headspace velocity was calculated to be 4.9–7.0 cm s^{-1}. Large variability in the measured headspace velocity suggests turbulent flow conditions in the wave channel, which is further supported by aerosol concentrations discussed later.

3.3 Characterization of particle backgrounds and SSA production

Background particle concentrations were measured in the wave channel headspace at the upstream sampling port (Fig. 1, Location 4) using a CPC to determine the contribution of non-marine particles from sources such as leaks in the paddle tent or breakthrough in the air handling system while the waves were being generated. Setting the RPM of the induction motor

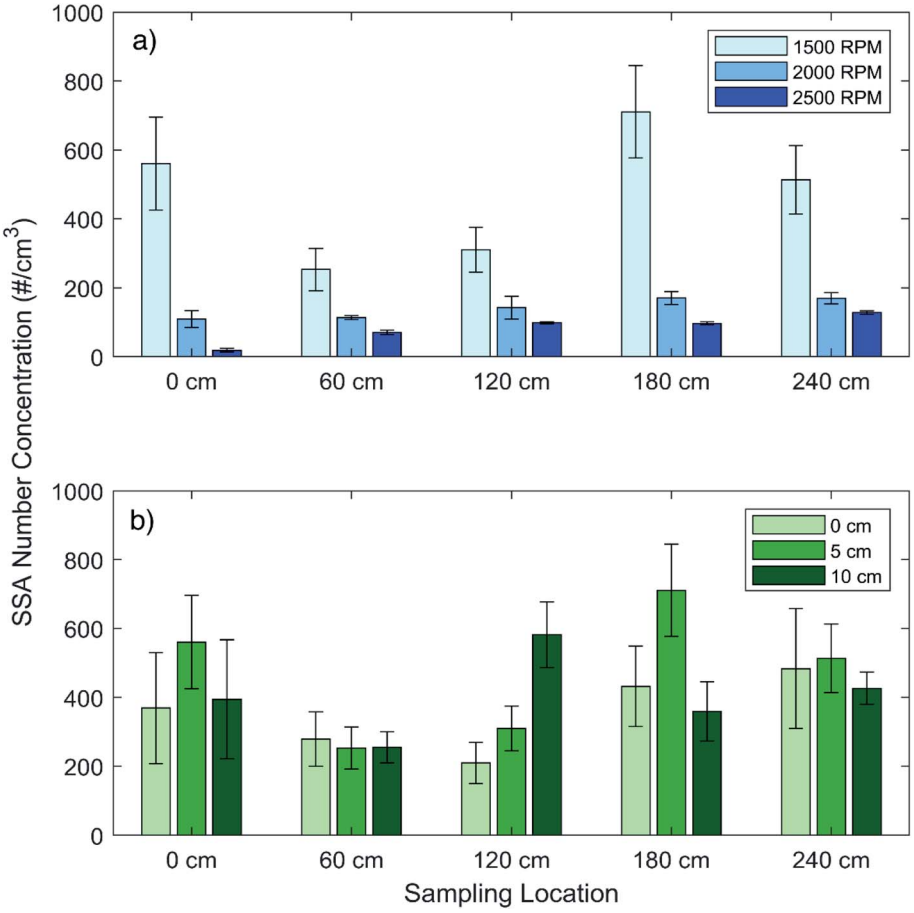

Fig. 5 (a) SSA number concentration measured at five sampling locations with a 5 cm port depth, testing three different fan settings, which control the air velocity in the wave channel headspace. The lowest setting (1500 RPM) was determined to yield the highest SSA concentrations at all sampling locations. (b) The SSA number concentrations at the different sampling locations with a fan speed of 1500 RPM, showing the effect of sampling port depth (0 cm, 5 cm, and 10 cm below the channel lids). There is no clear relationship between sampling port depth or location and number concentration, indicating heterogeneous particle concentrations in the channel headspace. The sampling port locations are evenly spaced and correspond to 0 cm, 60 cm, 120 cm, 180 cm, and 240 cm from the downstream end of the beach.

that supplied clean air to the wave channel to a speed less than 1500 RPM introduced ambient non-marine particles into the wave channel headspace (10–50× more than fan speeds greater than 1500 RPM), thus establishing a lower limit of the air handling unit. While increasing the speed of the motor could increase the amount of clean air into the headspace of the wave channel, doing so dilutes the total number of SSA from wave breaking. Thus, our testing found that 1500 RPM was the optimal fan speed (Fig. 5a and S4†) and this setting was used for all subsequent experiments.

With the optimized setting of the air handling unit, these background particle concentrations were generally low (~3 #/cm^3), indicating that the wave channel headspace was quite clean, with respect to ambient particulate contamination (~10 000 #/cm^3). In comparison, the average particle concentrations after the breaking wave were significantly higher (242 ± 91 #/cm^3), indicating that the vast majority (>98%) of the particles sampled downwind of the breaking wave were sea spray aerosols produced in the wave channel.

With the air handling unit and the background optimized, the next step was to optimize the sampling location for SSA downwind of the breaking waves. Five locations at 0 cm, 60 cm, 120 cm, 180 cm, and 240 cm downwind of the breaking wave were tested. Interestingly, the shape of the APS and SMPS size distributions do not change significantly between the different sampling locations, whereas the total particle concentrations do exhibit variability (Fig. S5†). Thus, the size distributions were used to calculate the total SSA number at each location. Fig. 5b shows that position 4, which corresponds to 180 cm downwind of the breaking waves, had the highest SSA number concentrations. The continuous water and air flows pushed the entrained air bubbles and the generated SSA downwind of the breaking wave.[3,8] In addition to sampling location, the sampling port (1.27 cm i.d.) depth was tested, from 0 cm to 10 cm into the headspace as measured from the lid panel. While the specific relationship between port depth and SSA number concentration varied with sampling location, at position 4, a port depth of 5 cm yielded the highest values. However, lack of clear trend in the total number concentration as a function of sampling location and depth indicates that there may be heterogeneous mixing within the wave channel headspace due to flow turbulence. In addition, factors such as wall losses and gravitational deposition of particles may have influenced the variability in particle numbers. It was observed during testing that sampling port depths of 10 cm or greater were prone to splashing by the breaking waves, resulting in water being pulled into the sampling lines. Similarly, a port depth of 0 cm (flush with the lid surface) resulted in condensation from the lids being pulled into the sampling lines. Thus, from an operational standpoint, a sampling port depth of 2–8 cm is ideal to minimize the introduction of water to the sampling lines.

4. Results from the SeaSCAPE experiment

4.1 Biological dynamics of phytoplankton blooms

While three distinct phytoplankton bloom experiments were performed during SeaSCAPE, results from the third bloom experiment will focused on in this manuscript due to the large amount of data taken during the full study. In addition, the most complete suite of measurements was taken during Bloom 3. The time series of seawater chl-a, heterotrophic bacteria, and dissolved organic carbon, shown in Fig. 2a, provide an overview of the biological progression of Bloom 3. Chl-a time series for Blooms 1 and 2 are shown in Fig. S6.† No significant phytoplankton growth was observed after the first nutrient addition (chl-a < 2 μg L^{-1}, Fig. 2a), possibly due to light limitation. A phytoplankton bloom was induced in an outdoor tank with natural seawater collected as before and then added to the wave channel on 8/1 (Table 1). After the addition of the outdoor-grown bloom, the phytoplankton growth continued and peaked at 25 μg L^{-1} chl-a, and then proceeded through an

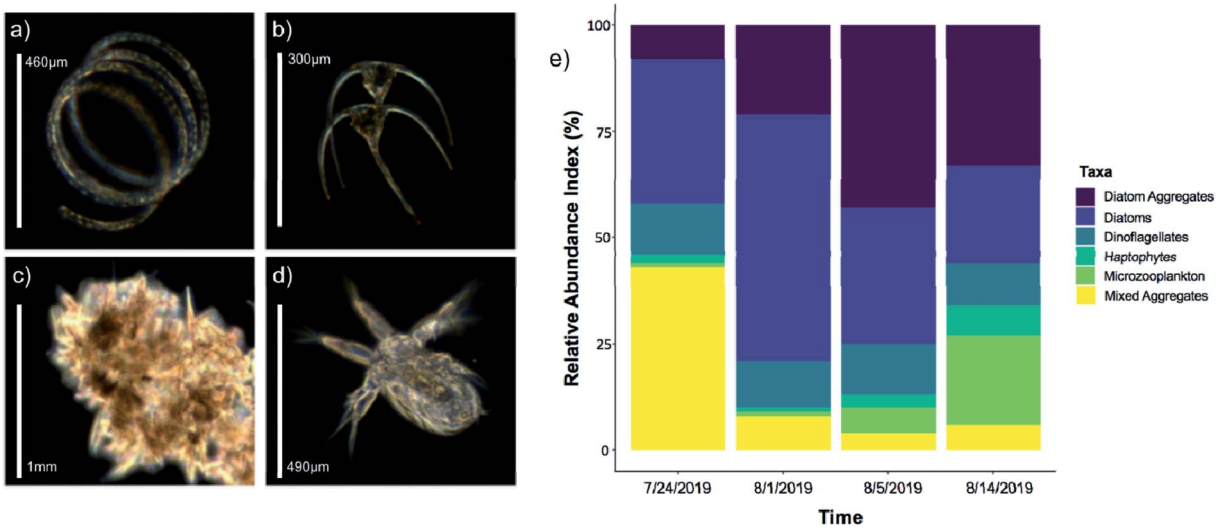

Fig. 6 Micrographs of representative taxa across Bloom 3 showing (a) diatoms; (b) dinoflagellates; (c) mixed aggregates (dominated by diatoms and haptophytes); (d) nauplius (microzooplankton), (e) time series of relative speciation of phytoplankton taxa across SeaSCAPE.

extended senescent phase (Fig. 2a). Following the peak of the bloom, chl-a concentrations remained stable around 5 μg L^{-1}, higher than the pre-bloom state, suggesting some phytoplankton growth was still occurring. Bacterial and viral dynamics (Fig. 2a) followed a typical microbial succession generally observed during phytoplankton bloom.[66]

The combination of *in situ* camera and inverted microscopy, along with chlorophyll concentrations over time, confirmed a distinct natural bloom progression in Bloom 3 (Fig. 6). Phytoplankton community structure was initially dominated by diatoms (composed mostly of *Skeletonema* sp. and *Cylindrotheca* sp.) with an overall relative abundance of 55% and 1.9×10^6 cells per L. The community then shifted towards an aggregation of diatoms (composed mostly of *Cylindrotheca* sp. and *Navicula* sp.) at the end of the bloom with a relative abundance of 33% and 5.0×10^5 cells per L. There was also a proliferation in microzooplankton (composed mostly of tintinnids and copepods) at the end of the bloom with a relative abundance of 25% and 5.452×10^3 cells per L. Phytoplankton physiology across the bloom was screened with both methods, and showed signs of pigment loss, broken frustules, and increased aggregation over time.

4.2 Temperature, relative humidity, dissolved gases, and DOC

Over the course of Bloom 3, dissolved organic carbon steadily increased in concentration, due to both primary production and bacterial production of DOC, which is consistent with previous bloom incubation experiments.[20] Notably, the addition of the outdoor tank resulted in a DOC increase of 100 μM compared to the background level of the first week. The dissolved inorganic gases, O_2 and CO_2, varied on a diurnal basis as the phytoplankton utilized light for photosynthesis and produced O_2 as a byproduct during the daytime. During periods of higher chl-a (Fig. 2a), after the outdoor tank amendment, dissolved O_2 concentrations were generally more elevated, except for 8/2 when the heterotrophic bacteria reached a local maximum concentration. The dissolved CO_2 concentration steadily decreased with respect to chl-a due to increased carbon fixation by phytoplankton. After reaching a minimum on 8/5 (Fig. 2b), the CO_2 concentration began increasing during the senescent phase of the mesocosm probably in response to increased bacterial respiration relative to carbon fixation by phytoplankton.

The seawater temperature of the wave channel initially began at the temperature of the ocean (17 °C) but equilibrated quickly to the temperature of the hydraulics laboratory within ~24 hours (Fig. 2b). Daily, temperature varied ~0.75 °C per day with the ambient temperature of the laboratory. Longer term variation in water temperature followed changes in local weather but ranged between 24.5-27 °C for the duration of experiment after initial equilibration. The air temperature and relative humidity in the wave channel headspace also exhibited a strong diurnal cycle (Fig. S7†). The mean air temperature during the campaign was 24 ± 1 °C and the relative humidity was 86 ± 5% (Table S2†). Keeping both the seawater and headspace air at controlled temperatures will be one of the key improvements of future setups to more accurately simulate real ocean conditions.

4.3 Impact of transportation and biological activity on seawater dissolved organic matter

Two selected analyses of DOM are shown here to illustrate various factors which influenced the seawater chemistry: the impact of (1) seawater transportation and (2) phytoplankton growth on the DOM composition. In order to fill the SIO wave channel, 11 800 L of seawater must be collected from the ocean and transported into the laboratory facility. Due to the handling of the seawater, there is concern that the process may introduce anthropogenic contaminants to the water. Fig. S8† is a GCxGC ion chromatogram of seawater obtained from the ocean before addition to the wave channel. Notable in the composition of this seawater is the vast chemical diversity of the sample, as well as a large number of known anthropogenic contaminants, such personal care products and plasticizers. These species are ubiquitous in the coastal zone and are unavoidable in mesocosm experiments using coastal seawater.[67,68]

To understand the effect of physical transport on the chemical composition of the seawater during SeaSCAPE, TD-GCxGC-EI-HRToFMS was performed on DOM samples from seawater gathered from the SIO pier before and after transfer to the wave channel on 7/23. As a comparison, we also analyzed DOM of the seawater after the addition of the outdoor phytoplankton culture on 8/1 to understand the influence of biological processes on DOM. Fig. 7a shows a spectral comparison plot in which the ion intensity chromatogram obtained after the water transfer was subtracted by the chromatogram obtained before the water was transferred. Within the limits of GCxGC sensitivity, we found that few compounds were introduced by the transfer process, with less than 4% of the ion current in the post transfer sample attributable to species classified as water transfer introduced contaminants (Fig. 7b). In contrast to the small changes made by water transfer, a much larger change was measured in DOM after the addition of the outdoor phytoplankton tank to the wave channel, with over 87% of the GCxGC signal introduced or significantly enhanced after the perturbation (Fig. 7b). This is likely due to organic material being actively produced by biological activity in the seawater. Thus, we find that transportation of the seawater to the wave channel has a relatively small effect on seawater composition, especially in contrast to the large changes induced by phytoplankton growth.

4.4 nSSA size distributions and stability

The shape of the nSSA size distributions is largely consistent with previous studies of SSA generated by breaking waves (Fig. S9†).[8] However, there was significant temporal variability in the total concentration of particles observed during the experiment. A strong diurnal trend was observed, with higher, more variable concentrations observed during the daytime ($N_{day} = 272 \pm 92$ #/cm^3) and lower, yet more stable concentrations observed during the nighttime ($N_{night} = 199 \pm 70$ #/cm^3) (Fig. 8). While seawater temperature can affect the flux of nSSA, the daily changes observed during the SeaSCAPE experiment were likely not large enough to explain the variability in nSSA concentration.[3] Typical daily water temperature changes were less 1 °C (Fig. 2), which should correspond to a change in SSA flux of only

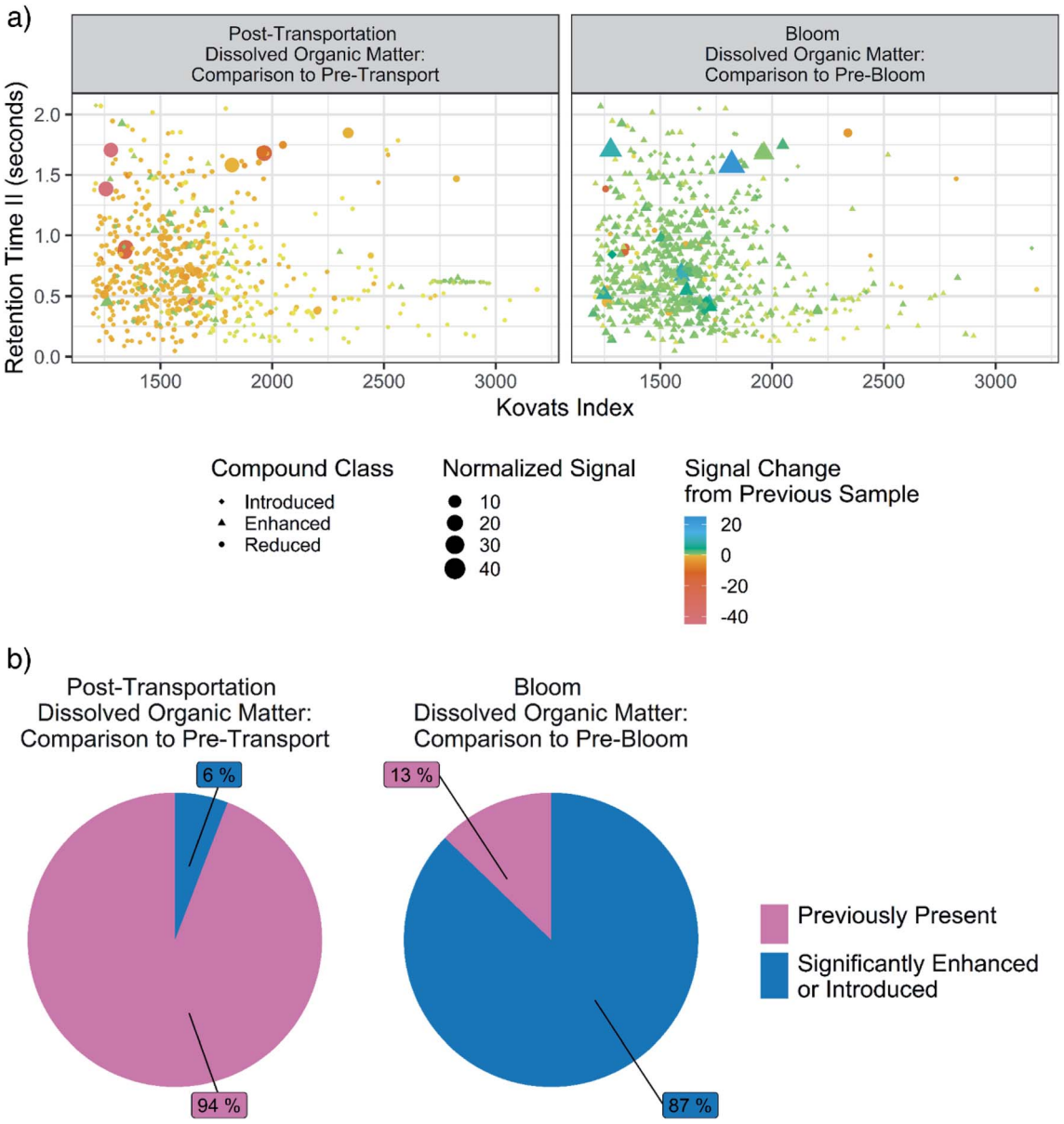

Fig. 7 (a) GCxGC spectra of DOM from Bloom 3, post-transportation from Scripps Pier into the wave channel (left) and post-bloom addition (right) samples illustrating the relative changes from pre-perturbation conditions. (b) Composition of DOM (semi-quantified by internal standard normalized GCxGC ion signal intensity) after physical water transport from Scripps Pier (left) and after introduction of the concentrated bloom addition of 8/1 (right), segregated by change relative to prior sample, with pink indicating signal attributable to previously present compounds and blue attributable to species that are newly introduced or significantly (>15%) enhanced in comparison to the prior signal.

2–4%,[69] whereas the observed change from night to day is, on average, ~37%. The diurnal changes also do not appear to be linked to other changes such as the wave channel lights, biological productivity, or the chemical composition of the seawater. Rather, we suspect that the changes in SSA production were driven by the opening and closing of the laboratory doors, which may have affected the air flow and mixing dynamics within the channel headspace. These findings, alongside the results of the sampling port location and depth testing (Fig. 5b), demonstrate the turbulent mixing within the wave channel headspace, resulting in variable nSSA number concentrations. Further testing and modelling studies of the wave channel are necessary to fully understand these observations.

4.5 Characteristics of hetSSA and SMA produced in the OFRs

OFRs were used to assess the effects of atmospheric aging on gases and particles emitted from the oceans. While the primary goal of the OFR1 and OFR2 experiments was to assess the effects of photooxidative aging on the properties of SSA (referred to as hetSSA herein), the gases present in the wave channel headspace were not removed and thus also reacted in the OFRs. New particle formation was observed due to the reactions of these gases, as evidenced by the appearance of a large nucleation mode in the aerosol distributions when the OFRs are active (Fig. 9a). The formation of SMA in OFR1 and OFR2, both as nucleated particles and *via* condensation onto SSA, presents

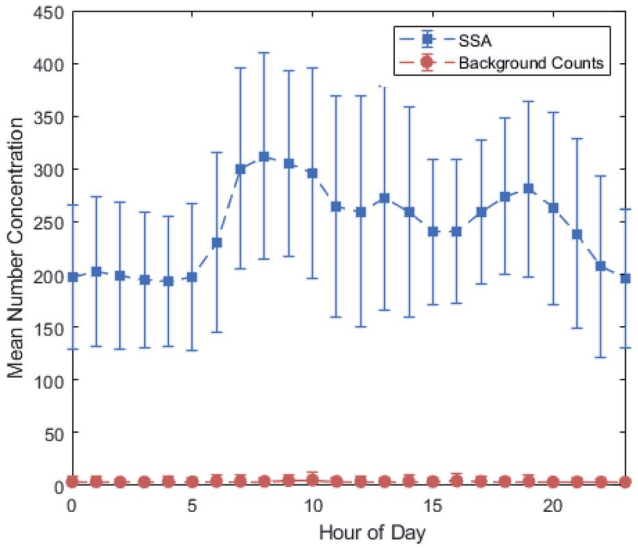

Fig. 8 Hourly average SSA number concentrations for all of Blooms 2 and 3, as measured by the APS and SMPS, demonstrating the variability in aerosol production, as well as the observed diurnal behavior. In general, particle concentrations tended to be higher and more variable during the daytime, but lower and more stable overnight. Background particle counts, as measured by the upstream CPC, are also shown. Times reflect local time (PST).

a significant challenge for the measurement of hetSSA. Size-resolved measurements can overcome this by simply selecting for particle sizes larger than the ultrafine mode (D_p > ~100 nm) and thus presumed to be primary SSA particles. These larger SSA particles may contain secondary species but will have also undergone heterogeneous oxidation by OH radical and ozone in the OFR. Measurements of the bulk non-refractory aerosol show significant changes in chemical composition due to oxidation processes in the OFR. In the bulk chemical speciation shown in Fig. 9, the relative increase in particulate nitrate, compared to non-refractory particulate chloride, is consistent with heterogeneous reaction of HNO_3 + NaCl → $NaNO_3$ + HCl.[70] The displacement of chloride for nitrate has been previously observed in coastal sea spray aerosol[71] and explored in laboratory experiments.[25,72] In our experiment, this anion substitution indicates that HNO_3 is likely produced in the OFR when sampling the wave channel head space air through the oxidation of NO_x to form HNO_3.

4.6 Evidence of abiotic volatile organic compound production from interfacial photochemistry

To test whether VOCs could be produced abiotically by irradiating the organic surface species with sunlight, surface water from the wave channel was exposed to light from a solar simulator and analyzed using a modified gas-phase APCI Orbitrap MS. Shown in Fig. 10a, two unique molecular signatures were significantly enhanced upon irradiation compared to other measured m/z signals, as well as three others not shown here (isoprene, dimethyl sulfone, and decadienal only in some days during Bloom 3). Several other species, many unidentified, also increased during this time but exhibited a more gradual

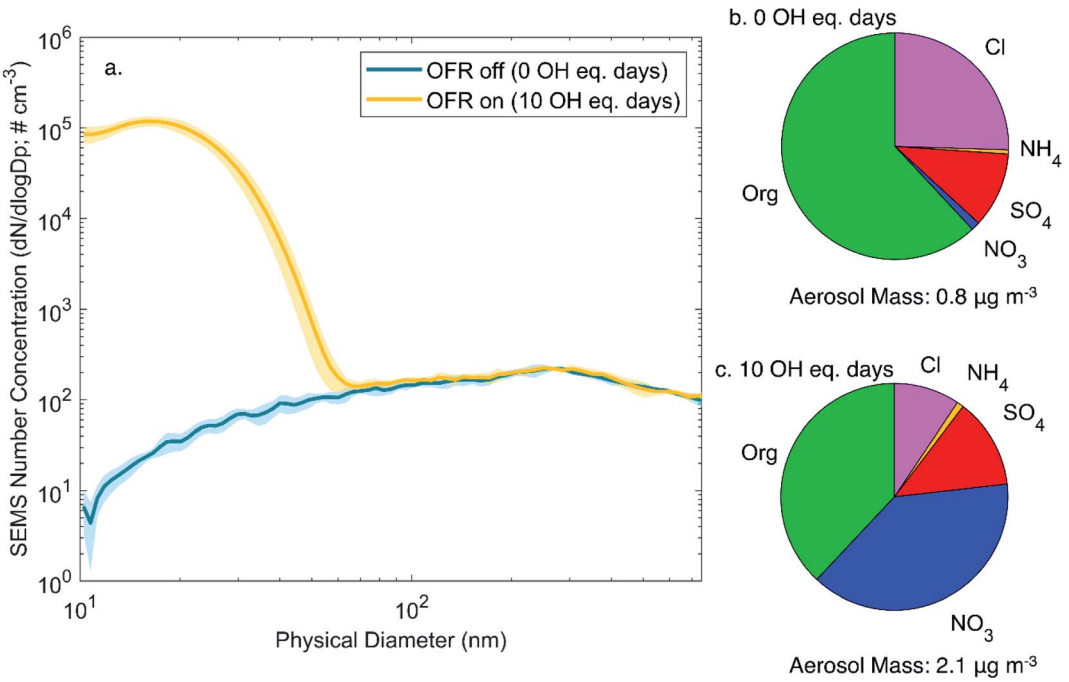

Fig. 9 Representative aerosol size distribution from OFR1 (a), in which the complete mixture of gases and SSA from the wave channel headspace are oxidized in the OFR. Shading represents variability in the particle concentrations during the sampling period (±1σ). The ultrafine mode at <100 nm, which is present only when the lamps are active, is evidence of new particle formation in the reactor. Median fractional bulk chemical composition of submicron non-refractory aerosol, as measured by the AMS, for (b) nascent/bypass SSA and (c) SSA aged 10 OH-equivalent days in the OFR. It is important to note that only a fraction of the total chloride is measured by the AMS.

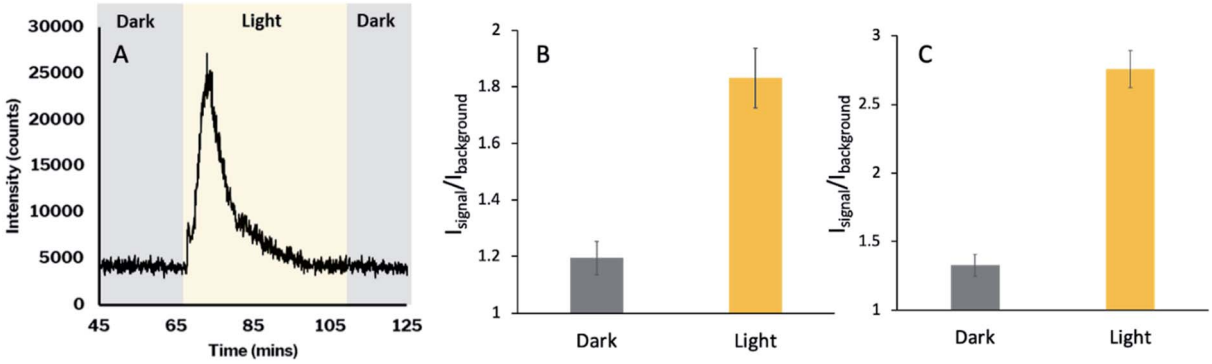

Fig. 10 Data from gas-phase APCI high resolution mass spectrometry showing (A) total ion current of summed volatile species found to be sensitive to irradiation, where gray indicates when the sample was kept dark and yellow when the sample was subjected to light; (B) the signal enhancement of C_6H_6O, likely phenol, upon irradiation, and (C) the signal enhancement of $C_{10}H_{16}O$, or beta-cyclocitral, upon irradiation. Error bars represent one standard deviation of the signal averaged over its highest peak.

increase, indicating a diffusion limited, and therefore most likely biogenic or non-surface related, process.[73,74] Two of these species, generated *via* irradiation, were annotated using tandem MS, showing fragmentation patterns that indicated the presence of phenol, C_6H_6O, and possibly beta-cyclocitral, $C_{10}H_{16}O$. The signal enhancement of these molecules immediately upon irradiation (within 3 minutes), compared to the background dark signal, are shown in Fig. 10b and c respectively. The fragmentation pattern of $C_{10}H_{16}O$ suggests that beta-cyclocitral was the dominant species with this mass-to-charge ratio, but multiple other isobaric species contributed a minor signal. Without an in-depth experiment to constrain the many variables in seawater such as the microbiology, including viruses and enzymes not removed by filtration, or surface tension, it is difficult to make any assumptions about the specific mechanisms responsible for photo-initiated VOC production. Only recently have studies begun to explore the mechanisms of interfacial VOC production at the ocean surface. Models and uncertainties in field measurements point towards a significant source of abiotic compounds.[73,75] Gas-phase APCI Orbitrap MS was shown to successfully ionize a variety of molecular signatures off-gassing from the seawater surface as well as detect changes when the sample was exposed to solar light.

4.7 Relative distribution of morphologies for nascent and hetSSA

Nascent SSA displayed four unique morphologies including prism-like, core–shell, rounded and aggregates, while hetSSA had two main morphologies: core–shell and rounded (Fig. 11a). The morphological categorization was performed qualitatively, analogous to previous studies.[23,76] Next, the relative distribution of morphologies for nSSA and hetSSA samples were compared (Fig. 11b). For the nSSA sample morphologies, the rounded (47%) was most common, followed by the core–shell (22%), while prism-like (17%) and aggregates (14%) showed similar abundancies. On the other hand, for the hetSSA sample morphologies, core–shell (72%) was most common, followed by the rounded (28%) morphology, while no prism-like and aggregates were observed. Overall, SSA aging results in significant increase of the abundance for core–shell morphology, and concomitant decreases in the other morphologies. Additionally, core–shell hetSSA particles showed a thicker coating compared with similar-size nascent core–shell particles.

5. Discussion

5.1 Wave channel characterization

A key challenge in ocean-atmosphere simulation experiments is maintaining the highest degree of experimental cleanliness while still capturing the complexity of the natural environment. This challenge is further pressed by the massive volumes of seawater that must be collected and transferred without significant perturbation of the biological assemblages and chemical contamination of the water. For the headspace, large airflows are necessary to offset the flow demand required by online instrumentation and filter sampling. Generating large volumes of high purity air is a significant challenge beyond the removal of particulates. Here we showed that the transfer of seawater from the ocean to the laboratory incurred little contamination; however, there was significant breakthrough of anthropogenic contaminants in the air handling system. The incorporation of the ISV was a critical addition that enabled the measurement of secondary marine aerosol and gases by generating a clean headspace for seawater VOCs to partition into. In the future, advances in economically generating high volumes of particle-free, ultrapure air would be ideal to enable the measurements of seawater-produced VOCs without the incorporation of secondary chambers.

Systematic testing of the wave channel was conducted to determine the optimal sampling conditions for nascent SSA. This testing showed a clear relationship between the air flow rate in the channel headspace and the measured concentrations of SSA particles, with lower air speeds resulting in higher particle concentrations. However, when the effect of both sampling port location and penetration depth into the channel headspace were evaluated, it was apparent that the nSSA concentrations in the headspace were heterogeneous

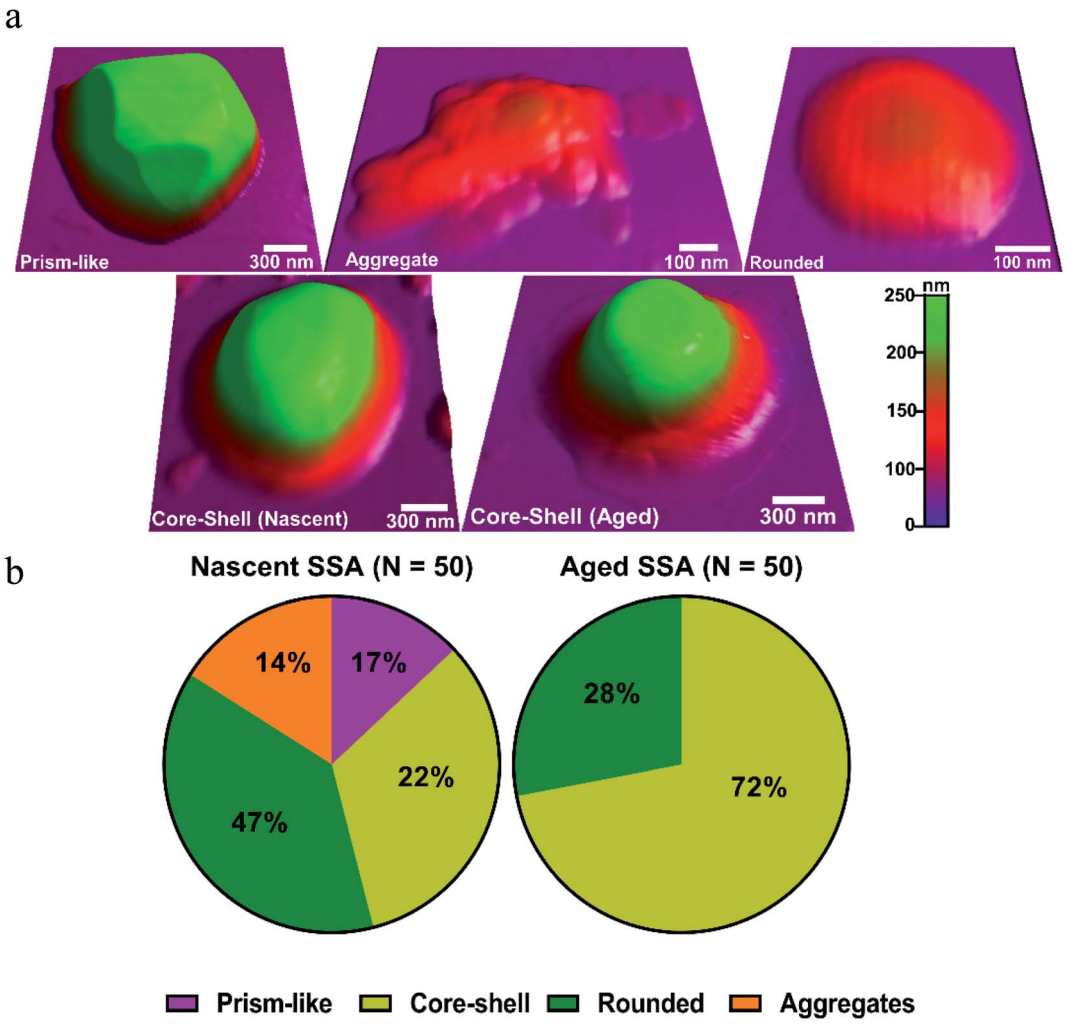

Fig. 11 (a) Representative AFM 3D-height images of individual SSA particles observed during the peak-bloom (Aug 3rd). Color scale shows height difference between the particles. (b) Relative distribution of the morphologies in nascent and aged SSA samples. Prism-like, core–shell, rounded, and aggregates particles are represented by purple, yellow, green, and orange colors, respectively.

and highly variable, depending on sampling locations. Further observations during the SeaSCAPE experiment showed a strong diurnal trend in the nSSA concentrations, which may have been caused by the opening and closing of the laboratory doors, creating a change in air pressure in the building. Based on these findings, future work is needed to model the fluid dynamics in the wave channel to understand the mixing and transport of aerosols and gases in the headspace. Additionally, it was observed that nSSA concentrations were typically more stable at night when the laboratory doors were closed, which reduced ambient air movement in the facility. This suggests that future modifications could be made to the wave channel to increase stability in the particle concentrations, such as replacing the open flap at the end of the channel with an improved vent system to control air flow. However, despite the variability in total number concentrations, the shape of the SSA size distributions remained consistent throughout the experiment and agrees well with previous wave channel experiments.[8] This indicates that the variability in the number concentrations was driven by different degrees of dilution, due to uneven mixing in the headspace, as opposed to variations in the SSA production mechanism or bubble sizes generated by the breaking wave.

5.2 Biological dynamics during the mesocosm experiment

One of the most crucial elements of mesocosm experiments to study ocean-atmosphere processes is the stimulation of a phytoplankton bloom, involving all the trophic interactions in the microbial loop between phytoplankton, protozoans, heterotrophic bacteria, and viruses.[32,66,77,78] Recent efforts have sought to better reproduce the complexity of marine biology while also accurately measuring the turnover of assemblages to better ascribe changes in seawater, SSA composition and properties, and VOC production. An ongoing challenge is the successful stimulation of authentic mesocosms using natural seawater, which varies in biological composition and may not respond immediately to nutrient amendments. During Bloom 3, the addition of the outdoor tank grown in elevated nutrient conditions and natural sunlight provided a richer starter culture for further growth in the wave channel. In the future,

enhanced lighting intensity, which more closely mimics natural sunlight, will be implemented to allow bloom formation without this added intervention.

The combination of SPCS and microscopy provided a detailed observation of the phytoplankton and microzooplankton dynamic and trophic interactions during the experiment. The phytoplankton assemblages showed a natural succession throughout the course of the experiment, from a diatom-dominated community at the peak of the bloom during the growth phase towards a diatom-aggregate and zooplankton-populated senescent phase. Observation of potential grazing on phytoplankton by microzooplankton and aggregate formation towards the end of the bloom provided insight on the physiological state of the phytoplankton bloom across the experiment (Fig. 6). These types of stressors upon phytoplankton may lead to released exudates containing carbon and sulfur that will supply microbial metabolisms, which in turn may influence the production and composition of climate relevant trace gases and the composition of biogenic aerosol.[79] Future work will compare phytoplankton and VOC concentrations across this study, to screen for specific taxa that may influence VOC production and transformation. The connections between the biological species and the chemical composition of DOM and aerosol will also be the focus of forthcoming SeaSCAPE studies. Further analysis of the functional (*e.g.* production, enzymes) and community (16S and 18S rDNA amplicon sequencing) adaptation of the marine microbes over the course of the bloom in the bulk seawater, SSML and aerosols will help address some of the chemical changes observed during SeaSCAPE.

5.3 Photochemical VOC production

The abiotic production of VOCs from seawater *via* reactions of surface-present organics with light and oxidants has been recently discussed as a possible source of atmospheric VOCs competitive in emission quantity with marine biology.[75] Currently, only laboratory measurements of abiotic VOC production have been undertaken, with most utilizing SSML or synthetic organic films doped with terrestrially relevant photosensitizers to enhance yields of irradiation-initiated VOC emission.[73,80] Here, using unadulterated seawater from our mesocosm experiments, we show small quantities of abiotic, light-driven VOC generation, including cyclic species, but do not maintain sustained emission compared to other laboratory investigations. Lack of sustained emission is likely due to the limited pool of volatile organic species in seawater, which may have been lost through emission and chemical transformation. While the complex mechanisms that control photoinitiated VOC production are poorly understood, mesocosm experiments serve as a valuable bridge between field and laboratory work towards determining the relative contributions of biotic and abiotic VOC production in the marine environment and will be further pursued.

5.4 Influence of photochemical aging on SSA composition and secondary aerosol formation

Small SSA can be significantly enriched with organic species,[81] which influences their reactivity and water uptake properties.[24,82] However, the role of atmospheric oxidation processes in transforming the organic chemical composition of SSA remains poorly understood. We found that heterogeneous aging of SSA by OH radical led to significant changes in its morphology, with the total loss of prism-like and aggregate type particles and a large enhancement in core–shell particles. Increased oxidation of organic aerosol has been shown to increase its viscosity, potentially affecting its phase state.[83,84] This process may have contributed to the change in SSA morphologies observed here. An alternative explanation is that coating of secondary organic species onto the SSA altered its morphology. Future studies are necessary to understand how both of these processes influence SSA phase and morphology, and the potential influence on the climate relevant properties of SSA, such as ice nucleation, water uptake, and light scattering.

6. Conclusions

In summary, wave channels are an important method for understanding the production and properties of marine aerosols and gases under controlled laboratory conditions. Optimization of the wave channel system has enabled even more detailed atmospheric measurements over previous experimental campaigns. In addition, major improvements have been made in the capability to simulate complex seawater biology. The incorporation of oxidation flow reactors has, for the first time, enabled the study of secondary aerosol formation and photochemical aging of SSA during a large-scale wave channel experiment. Preliminary findings from the SeaSCAPE campaign shed light on the photochemical production of VOCs, impact of atmospheric aging on SSA phase and morphology, and the chemical composition of SMA. Future analysis of the SeaSCAPE dataset is expected to give insight to, among other processes, the nature of marine INPs in both freshly emitted and hetSSA; the potential for both SSA and SMA to serve as CCN in the marine atmosphere; the molecular composition of SSA and its links to biological activity; the identity of unique marine VOCs and possible SOA precursors; and the effect of photochemical aging on the chemical composition of marine aerosols. Oceanic emissions of both gases and particles have profound effects on the climate through their interactions with clouds and solar radiation. Laboratory ocean-atmosphere experiments have and will continue to expand our knowledge of marine aerosols and their influence on a changing climate system.

Author contributions

J. S. S., K. J. M, C. L., V. H. G., T. H. B., C. D. C., and K. A. P. conceptualized the experiment. Investigation was conducted by J. S. S., K. J. M, C. L., M. R. A., S. A., C. J. B., E. B. F., D. R. C., D. D., J. D., L. A. G., C. P. K., D. B. K., L. E. M., B. A. M., D. R. M., C. K. M., A. N. M., C. A. M., C. M. N., M. A. P., D. P., R. M. C. S., S. S., P. R. T., J. L. W., F. M., and C. D. C. Project administration was performed by C. L. Supervision of the project was conducted by P. J. D., D. K. F., A. H. G., V. H. G., J. S. J., F. M., T. R. M., J. H. S., A. V. T., T. H. B., C. D. C., and K. A. P. The original draft of the manuscript was written by J. SS., K. J. M, C. L., M. R. A., S. A., E.

B. F., D. R. C., J. D., L. A. G., C. P. K., D. B. K., L. E. M., B. A. M., C. K. M., M. A. P., P. R. T., J. L. W., F. M. The paper was reviewed and edited by D. P., R. M. C. S., P. J. D., D. K. F., A. H. G., V. H. G., J. H. S., A. V. T., T. H. B., C. D. C., K. A. P.

Conflicts of interest

There are no conflicts to declare.

Acknowledgements

This material is based upon work supported by the National Science Foundation through the NSF Center for Aerosol Impacts on the Chemistry of the Environment, a Center for Chemical Innovation (CHE-1801971). Thank you to the entire SeaSCAPE team for their hard work throughout the experimental campaign. A full list of participants can be found online: https://caice.ucsd.edu/experiment-campaigns/. We thank Tran Nguyen and the Professor Lihini Aluwihare Lab for analysis of the DOC samples. We would like to acknowledge Dr Pedro Belda-Ferre, Professors Elizabeth Stone, Juan Navea, Mike Tauber, Jim Smith, Pieter Dorrestein, Rob Knight, and Farooq Azam for their contributions to the experiment. Special thanks to Joe Mayer for his assistance with fabricating the ISV and the wave channel paddle system; Professor Mark Young for assisting with the paddle software; Dr Grant Deane and Dr Dale Stokes for assistance with wave channel operation; and Rob Klidy and the Hydraulics Laboratory staff. Thank you to Dr Victor Or for designing the TOC graphic.

References

1 O. Boucher, D. Randall, P. Artaxo, C. Bretherton, G. Feingold, P. Forster, V. M. Kerminen, Y. Kondo, H. Liao, U. Lohmann, P. Rasch, S. K. Satheesh, S. Sherwood, B. Stevens and X. Y. Zhang, Clouds and Aerosols, in *Climate Change 2013: The Physical Science Basis. Contribution of Working Group I to the Fifth Assessment Report of the Intergovernmental Panel on Climate Change*, ed. T. F. Stocker, D. Qin, G.-K. Plattner, M. Tignor, S. K. Allen, J. Boschung, A. Nauels, Y. Xia, V. Bex and P. M. Midgley, Cambridge University Press, Cambridge, United Kingdom and New York, NY, USA, 2013, pp. 571–632.

2 K. S. Carslaw, L. a. Lee, C. L. Reddington, K. J. Pringle, A. Rap, P. M. Forster, G. W. Mann, D. V. Spracklen, M. T. Woodhouse, L. A. Regayre and J. R. Pierce, Large Contribution of Natural Aerosols to Uncertainty in Indirect Forcing, *Nature*, 2013, **503**, 67–71.

3 E. R. Lewis and S. E. Schwartz, *Sea Salt Aerosol Production: Mechanisms, Methods, Measurements, and Models–A Critical Review; American Geophysical Union*, Washington D.C., 2004.

4 S. L. Gong, L. A. Barrie and M. Lazare, Canadian Aerosol Module (CAM): A Size-Segregated Simulation of Atmospheric Aerosol Processes for Climate and Air Quality Models 2. Global Sea-Salt Aerosol and Its Budgets, *J. Geophys. Res.: Atmos.*, 2002, **107**, 1–14.

5 X. Wang, G. B. Deane, K. A. Moore, O. S. Ryder, M. D. Stokes, C. M. Beall, D. B. Collins, M. V. Santander, S. M. Burrows, C. M. Sultana and K. A. Prather, The Role of Jet and Film Drops in Controlling the Mixing State of Submicron Sea Spray Aerosol Particles, *Proc. Natl. Acad. Sci. U. S. A.*, 2017, **114**, 6978–6983.

6 P. K. Quinn, D. B. Collins, V. H. Grassian, K. A. Prather and T. S. Bates, Chemistry and Related Properties of Freshly Emitted Sea Spray Aerosol, *Chem. Rev.*, 2015, **115**, 4383–4399.

7 C. D. O'Dowd and G. de Leeuw, Marine Aerosol Production: A Review of the Current Knowledge, *Philos. Trans. R. Soc., A*, 2007, **365**, 1753–1774.

8 K. A. Prather, T. H. Bertram, V. H. Grassian, G. B. Deane, M. D. Stokes, P. J. Demott, L. I. Aluwihare, B. P. Palenik, F. Azam, J. H. Seinfeld, R. C. Moffet, M. J. Molina, C. D. Cappa, F. M. Geiger, G. C. Roberts, L. M. Russell, A. P. Ault, J. Baltrusaitis, D. B. Collins, C. E. Corrigan, L. a Cuadra-Rodriguez, C. J. Ebben, S. D. Forestieri, T. L. Guasco, S. P. Hersey, M. J. Kim, W. F. Lambert, R. L. Modini, W. Mui, B. E. Pedler, M. J. Ruppel, O. S. Ryder, N. G. Schoepp, R. C. Sullivan and D. Zhao, Bringing the Ocean into the Laboratory to Probe the Chemical Complexity of Sea Spray Aerosol, *Proc. Natl. Acad. Sci. U. S. A.*, 2013, **110**, 7550–7555.

9 M. D. Stokes, G. B. Deane, K. Prather, T. H. Bertram, M. J. Ruppel, O. S. Ryder, J. M. Brady and D. Zhao, A Marine Aerosol Reference Tank System as a Breaking Wave Analogue for the Production of Foam and Sea-Spray Aerosols, *Atmos. Meas. Tech.*, 2013, **6**, 1085–1094.

10 M. D. Stokes, G. Deane, D. B. Collins, C. Cappa, T. Bertram, A. Dommer, S. Schill, S. Forestieri and M. Survilo, A Miniature Marine Aerosol Reference Tank (MiniMART) as a Compact Breaking Wave Analogue, *Atmos. Meas. Tech.*, 2016, **9**, 4257–4267.

11 E. Fuentes, H. Coe, D. Green, G. De Leeuw and G. McFiggans, On the Impacts of Phytoplankton-Derived Organic Matter on the Properties of the Primary Marine Aerosol – Part 1: Source Fluxes, *Atmos. Chem. Phys.*, 2010, **10**, 9295–9317.

12 K. Sellegri, C. D. O'Dowd, Y. J. Yoon, S. G. Jennings and G. de Leeuw, Surfactants and Submicron Sea Spray Generation, *J. Geophys. Res.: Atmos.*, 2006, **111**, 1–12.

13 K. A. H. Hultin, E. D. Nilsson, R. Krejci, E. M. Mrtensson, M. Ehn, Å. Hagström and G. De Leeuw, In Situ Laboratory Sea Spray Production during the Marine Aerosol Production 2006 Cruise on the Northeastern Atlantic Ocean, *J. Geophys. Res.: Atmos.*, 2010, **115**, 1–19.

14 S. Christiansen, M. E. Salter, E. Gorokhova, Q. T. Nguyen and M. Bilde, Sea Spray Aerosol Formation: Laboratory Results on the Role of Air Entrainment, Water Temperature, and Phytoplankton Biomass, *Environ. Sci. Technol.*, 2019, **53**(22), 13107–13116.

15 M. E. Salter, E. D. Nilsson, A. Butcher and M. Bilde, On the Seawater Temperature Dependence of the Sea Spray Aerosol Generated by a Continuous Plunging Jet, *J. Geophys. Res.*, 2014, **119**, 9052–9072.

16 D. B. Collins, D. F. Zhao, M. J. Ruppel, O. Laskina, J. R. Grandquist, R. L. Modini, M. D. Stokes, L. M. Russell, T. H. Bertram, V. H. Grassian, G. B. Deane and K. A. Prather, Direct Aerosol Chemical Composition Measurements to Evaluate the Physicochemical Differences between Controlled Sea Spray Aerosol Generation Schemes, *Atmos. Meas. Tech.*, 2014, **7**, 3667–3683.

17 K. J. Mayer, J. S. Sauer, J. Dinasquet and K. A. Prather, CAICE Studies: Insights from a Decade of Ocean – Atmosphere Experiments in the Laboratory, *Acc. Chem. Res.*, 2020, **53**, 2510–2520.

18 P. J. DeMott, T. C. J. Hill, C. S. McCluskey, K. A. Prather, D. B. Collins, R. C. Sullivan, M. J. Ruppel, R. H. Mason, V. E. Irish, T. Lee, C. Y. Hwang, T. S. Rhee, J. R. Snider, G. R. McMeeking, S. Dhaniyala, E. R. Lewis, J. J. B. Wentzell, J. Abbatt, C. Lee, C. M. Sultana, A. P. Ault, J. L. Axson, M. Diaz Martinez, I. Venero, G. Santos-Figueroa, M. D. Stokes, G. B. Deane, O. L. Mayol-Bracero, V. H. Grassian, T. H. Bertram, A. K. Bertram, B. F. Moffett and G. D. Franc, Sea Spray Aerosol as a Unique Source of Ice Nucleating Particles, *Proc. Natl. Acad. Sci. U. S. A.*, 2015, **113**, 201514034.

19 J. M. Michaud, L. R. Thompson, D. Kaul, J. L. Espinoza, R. A. Richter, Z. Z. Xu, C. Lee, K. M. Pham, C. M. Beall, F. Malfatti, F. Azam, R. Knight, M. D. Burkart, C. L. Dupont and K. A. Prather, Taxon-Specific Aerosolization of Bacteria and Viruses in an Experimental Ocean-Atmosphere Mesocosm, *Nat. Commun.*, 2018, 9.

20 X. Wang, C. M. Sultana, J. Trueblood, T. C. J. Hill, F. Malfatti, C. Lee, O. Laskina, K. A. Moore, C. M. Beall, C. S. McCluskey, G. C. Cornwell, Y. Zhou, J. L. Cox, M. A. Pendergraft, M. V. Santander, T. H. Bertram, C. D. Cappa, F. Azam, P. J. DeMott, V. H. Grassian and K. A. Prather, Microbial Control of Sea Spray Aerosol Composition: A Tale of Two Blooms, *ACS Cent. Sci.*, 2015, **1**, 124–131.

21 M. J. Kim, J. M. Michaud, R. Williams, B. P. Sherwood, R. Pomeroy, F. Azam, M. Burkart and T. H. Bertram, Bacterial-Driven Production of Nitrates in Seawater, *Geophys. Res. Lett.*, 2015, **42**, 1–8.

22 J. P. Patterson, D. B. Collins, J. M. Michaud, J. L. Axson, C. M. Sultana, T. Moser, A. C. Dommer, J. Conner, V. H. Grassian, M. D. Stokes, G. B. Deane, J. E. Evans, M. D. Burkart, K. A. Prather and N. C. Gianneschi, Sea Spray Aerosol Structure and Composition Using Cryogenic Transmission Electron Microscopy, *ACS Cent. Sci.*, 2016, **2**, 40–47.

23 H. D. Lee, S. Wigley, C. Lee, V. W. Or, E. S. Hasenecz, E. A. Stone, V. H. Grassian, K. A. Prather and A. V. Tivanski, Physicochemical Mixing State of Sea Spray Aerosols: Morphologies Exhibit Size Dependence, *ACS Earth Space Chem.*, 2020, **4**, 1604–1611.

24 O. S. Ryder, N. R. Campbell, H. Morris, S. Forestieri, M. J. Ruppel, C. Cappa, A. Tivanski, K. Prather and T. H. Bertram, Role of Organic Coatings in Regulating N_2O_5 Reactive Uptake to Sea Spray Aerosol, *J. Phys. Chem. A*, 2015, **119**, 11683–11692.

25 A. P. Ault, T. L. Guasco, O. S. Ryder, J. Baltrusaitis, L. A. Cuadra-Rodriguez, D. B. Collins, M. J. Ruppel, T. H. Bertram, K. A. Prather and V. H. Grassian, Inside *versus* Outside: Ion Redistribution in Nitric Acid Reacted Sea Spray Aerosol Particles as Determined by Single Particle Analysis, *J. Am. Chem. Soc.*, 2013, **135**, 14528–14531.

26 J. V. Trueblood, A. D. Estillore, C. Lee, J. A. Dowling, K. A. Prather and V. H. Grassian, Heterogeneous Chemistry of Lipopolysaccharides with Gas-Phase Nitric Acid: Reactive Sites and Reaction Pathways, *J. Phys. Chem. A*, 2016, **120**, 6444–6450.

27 A. D. Estillore, J. V. Trueblood and V. H. Grassian, Atmospheric Chemistry of Bioaerosols: Heterogeneous and Multiphase Reactions with Atmospheric Oxidants and Other Trace Gases, *Chem. Sci.*, 2016, **7**, 6604–6616.

28 J. V. Trueblood, X. Wang, V. W. Or, M. R. Alves, M. V. Santander, K. A. Prather and V. H. Grassian, The Old and the New: Aging of Sea Spray Aerosol and Formation of Secondary Marine Aerosol through OH Oxidation Reactions, *ACS Earth Space Chem.*, 2019, **3**, 2307–2314.

29 K. J. Mayer, X. Wang, M. V. Santander, B. A. Mitts, J. S. Sauer, C. M. Sultana, C. D. Cappa and K. A. Prather, Secondary Marine Aerosol Plays a Dominant Role over Primary Sea Spray Aerosol in Cloud Formation, *ACS Cent. Sci.*, 2020, **6**, 2259–2266.

30 S. R. Schneider, D. B. Collins, C. Y. Lim, L. Zhu and J. P. D. Abbatt, Formation of Secondary Organic Aerosol from the Heterogeneous Oxidation by Ozone of a Phytoplankton Culture, *ACS Earth Space Chem.*, 2019, **3**, 2298–2306.

31 M. Bouvet, N. Hoepffner and M. D. Dowell, Parameterization of a Spectral Solar Irradiance Model for the Global Ocean Using Multiple Satellite Sensors, *J. Geophys. Res.: Solid Earth*, 2002, **107**, 8–18.

32 C. Lee, C. M. Sultana, D. B. Collins, M. V. Santander, J. L. Axson, F. Malfatti, G. C. Cornwell, J. R. Grandquist, G. B. Deane, M. D. Stokes, F. Azam, V. H. Grassian and K. a. Prather, Advancing Model Systems for Fundamental Laboratory Studies of Sea Spray Aerosol Using the Microbial Loop, *J. Phys. Chem. A*, 2015, 150805131932006.

33 R. R. L. Guillard and J. H. Ryther, Studies of Marine Planktonic Diatoms, *Can. J. Microbiol.*, 1962, **8**, 229–238.

34 E. Kang, M. J. Root and W. H. Brune, Introducing the Concept of Potential Aerosol Mass (PAM), *Atmos. Chem. Phys.*, 2007, **7**, 5727–5744.

35 A. T. Lambe, A. T. Ahern, L. R. Williams, J. G. Slowik, J. P. S. Wong, J. P. D. Abbatt, W. H. Brune, N. L. Ng, J. P. Wright, D. R. Croasdale, D. R. Worsnop, P. Davidovits and T. B. Onasch, Characterization of Aerosol Photooxidation Flow Reactors: Heterogeneous Oxidation, Secondary Organic Aerosol Formation and Cloud Condensation Nuclei Activity Measurements, *Atmos. Meas. Tech.*, 2011, **4**, 445–461.

36 W.-C. Chen and R. A. Marcus, On the Theory of the Reaction Rate of Vibrationally Excited CO Molecules with OH Radicals, *J. Chem. Phys.*, 2006, **124**, 024306.
37 G. M. Wolfe, J. M. Nicely, J. M. S. Clair, T. F. Hanisco, J. Liao, L. D. Oman, W. B. Brune, D. Miller, A. Thames, G. González Abad, T. B. Ryerson, C. R. Thompson, J. Peischl, K. McKain, C. Sweeney, P. O. Wennberg, M. Kim, J. D. Crounse, S. R. Hall, K. Ullmann, G. Diskin, P. Bui, C. Chang and J. Dean-Day, Mapping Hydroxyl Variability throughout the Global Remote Troposphere *via* Synthesis of Airborne and Satellite Formaldehyde Observations, *Proc. Natl. Acad. Sci. U. S. A.*, 2019, **116**, 11171–11180.
38 H. D. Lee, C. P. Kaluarachchi, E. S. Hasenecz, J. Z. Zhu, E. Popa, E. A. Stone and A. V. Tivanski, Effect of Dry or Wet Substrate Deposition on the Organic Volume Fraction of Core–Shell Aerosol Particles, *Atmos. Meas. Tech.*, 2019, **12**, 2033–2042.
39 H. D. Lee, H. S. Morris, O. Laskina, C. M. Sultana, C. Lee, T. Jayarathne, J. L. Cox, X. Wang, E. S. Hasenecz, P. J. Demott, T. H. Bertram, C. D. Cappa, E. A. Stone, K. A. Prather, V. H. Grassian and A. V. Tivanski, Organic Enrichment, Physical Phase State, and Surface Tension Depression of Nascent Core–Shell Sea Spray Aerosols during Two Phytoplankton Blooms, *ACS Earth Space Chem.*, 2020, **4**, 650–660.
40 P. F. DeCarlo, J. R. Kimmel, A. Trimborn, M. J. Northway, J. T. Jayne, A. C. Aiken, M. Gonin, K. Fuhrer, T. Horvath, K. S. Docherty, D. R. Worsnop and J. L. Jimenez, Field-Deployable, High-Resolution, Time-of-Flight Aerosol Mass Spectrometer, *Anal. Chem.*, 2006, **78**, 8281–8289.
41 J. P. Kercher, T. P. Riedel and J. A. Thornton, Chlorine Activation by N_2O_5: Simultaneous, *in situ* Detection of ClNO2 and N2O5 by Chemical Ionization Mass Spectrometry, *Atmos. Meas. Tech.*, 2009, **2**, 193–204.
42 M. J. Kim, M. C. Zoerb, N. R. Campbell, K. J. Zimmermann, B. W. Blomquist, B. J. Huebert and T. H. Bertram, Revisiting Benzene Cluster Cations for the Chemical Ionization of Dimethyl Sulfide and Select Volatile Organic Compounds, *Atmos. Meas. Tech.*, 2016, **9**, 1473–1484.
43 A. Lavi, M. P. Vermeuel, G. A. Novak and T. H. Bertram, The Sensitivity of Benzene Cluster Cation Chemical Ionization Mass Spectrometry to Select Biogenic Terpenes, *Atmos. Meas. Tech.*, 2018, **11**, 3251–3262.
44 J. Krechmer, F. Lopez-Hilfiker, A. Koss, M. Hutterli, C. Stoermer, B. Deming, J. Kimmel, C. Warneke, R. Holzinger, J. Jayne, D. Worsnop, K. Fuhrer, M. Gonin and J. De Gouw, Evaluation of a New Reagent-Ion Source and Focusing Ion-Molecule Reactor for Use in Proton-Transfer-Reaction Mass Spectrometry, *Anal. Chem.*, 2018, **90**, 12011–12018.
45 M. Roveretto, M. Li, N. Hayeck, M. Brüggemann, C. Emmelin, S. Perrier and C. George, Real-Time Detection of Gas-Phase Organohalogens from Aqueous Photochemistry Using Orbitrap Mass Spectrometry, *ACS Earth Space Chem.*, 2019, **3**, 329–334.
46 L. E. Hatch, C. N. Jen, N. M. Kreisberg, V. Selimovic, R. J. Yokelson, C. Stamatis, R. A. York, D. Foster, S. L. Stephens, A. H. Goldstein and K. C. Barsanti, Highly Speciated Measurements of Terpenoids Emitted from Laboratory and Mixed-Conifer Forest Prescribed Fires, *Environ. Sci. Technol.*, 2019, **53**, 9418–9428.
47 D. J. Carlson, Surface Microlayer Phenolic Enrichments Indicate Sea Surface Slicks, *Nature*, 1982, **296**, 426–429.
48 M. Cunliffe and O. Wurl, Sampling the Sea Surface Microlayer, in *Hydrocarbon and Lipid Microbiology Protocols. Springer Protocols Handbooks*, ed. T. McGenity, K. Timmis and B. Nogales, Springer, Berlin, Heidelberg, 2015.
49 D. R. Worton, M. Decker, G. Isaacman-VanWertz, A. W. H. Chan, K. R. Wilson and A. H. Goldstein, Improved Molecular Level Identification of Organic Compounds Using Comprehensive Two-Dimensional Chromatography, Dual Ionization Energies and High Resolution Mass Spectrometry, *Analyst*, 2017, **142**, 2395–2403.
50 O. Holm-Hansen, C. J. Lorenzen, R. W. Holmes and J. D. H. Strickland, Fluorometric Determination of Chlorophyll, *J. Cons., Cons. Int. Explor. Mer*, 1965, **30**, 3–15.
51 D. W. Menzel and R. F. Vaccaro, The Measurement of Dissolved Organic Carbon in Seawater, *Limnol. Oceanogr.*, 1964, **9**, 138–142.
52 von H. Utermöhl, Neue Wege in Der Quantitativen Erfassung Des Plankton. (Mit Besonderer Berücksichtigung Des Ultraplanktons), *Verh. – Int. Ver. Theor. Angew. Limnol.*, 1931, **5**, 567–596.
53 E. C. Orenstein, D. Ratelle, C. Briseño-Avena, M. Carter, P. J. S. Franks, J. S. Jaffe and P. L. D. Roberts, The Scripps Plankton Camera System: A Framework and Platform for *in Situ* Microscopy, *Limnol. Oceanogr.: Methods*, 2020, **18**, 681–695.
54 J. M. Gasol and P. A. Del Giorgio, Using Flow Cytometry for Counting Natural Planktonic Bacteria and Understanding the Structure of Planktonic Bacterial Communities, *Sci. Mar.*, 2000, **64**, 197–224.
55 C. P. D. Brussaard, Optimization of Procedures for Counting Viruses by Flow Cytometry, *Appl. Environ. Microbiol.*, 2004, **70**, 1506–1513.
56 D. Marie, F. Partensky, S. Jacquet and D. Vaulot, Enumeration and Cell Cycle Analysis of Natural Populations of Marine Picoplankton by Flow Cytometry Using the Nucleic Acid Stain SYBR Green I, *Appl. Environ. Microbiol.*, 1997, **63**, 186–193.
57 R. T. Noble and J. A. Fuhrman, Use of SYBR Green I for Rapid Epifluorescence Counts of Marine Viruses and Bacteria, *Aquat. Microb. Ecol.*, 1998, **14**, 113–118.
58 R. J. Olson, S. W. Chisholm, E. R. Zettler and E. V. Armbrust, Pigments, Size, and Distributions of Synechococcus in the North Atlantic and Pacific Oceans, *Limnol. Oceanogr.*, 1990, **35**, 45–58.
59 S. V. Hering, S. R. Spielman and G. S. Lewis, Moderated, Water-Based, Condensational Particle Growth in a Laminar Flow, *Aerosol Sci. Technol.*, 2014, **48**, 401–408.
60 D. Marie, F. Rigaut-Jalabert and D. Vaulot, An Improved Protocol for Flow Cytometry Analysis of Phytoplankton

Cultures and Natural Samples, *Cytometry, Part A*, 2014, **85**, 962–968.

61 U. Christaki, C. Courties, R. Massana, P. Catala, P. Lebaron, J. M. Gasol and M. V. Zubkov, Optimized Routine Flow Cytometric Enumeration of Heterotrophic Flagellates Using SYBR Green I, *Limnol. Oceanogr.: Methods*, 2011, **9**, 329–339.

62 C. Ye, X. Zhou, D. Pu, J. Stutz, J. Festa, M. Spolaor, C. Tsai, C. Cantrell, R. L. Mauldin, T. Campos, A. Weinheimer, R. S. Hornbrook, E. C. Apel, A. Guenther, L. Kaser, B. Yuan, T. Karl, J. Haggerty, S. Hall, K. Ullmann, J. N. Smith, J. Ortega and C. Knote, Rapid Cycling of Reactive Nitrogen in the Marine Boundary Layer, *Nature*, 2016, **532**, 489–491.

63 J. H. Seinfeld and S. N. Pandis *Atmospheric Chemistry and Physics: From Air Pollution to Climate Change*, John Wiley & Sons, Inc., Hoboken, New Jersey, 3rd edn, 2016.

64 P. Boylan, D. Helmig and S. Oltmans, Ozone in the Atlantic Ocean Marine Boundary Layer, *Elem. Sci. Anthr.*, 2015, **3**, 1–13.

65 S. G. Wakeham, E. A. Canuel and P. H. Doering, Geochemistry of Volatile Organic Compounds in Seawater: Mesocosm Experiments with 14C-Model Compounds, *Geochim. Cosmochim. Acta*, 1986, **50**, 1163–1172.

66 A. Buchan, G. R. LeCleir, C. A. Gulvik and J. M. González, Master Recyclers: Features and Functions of Bacteria Associated with Phytoplankton Blooms, *Nat. Rev. Microbiol.*, 2014, **12**, 686–698.

67 L. Hermabessiere, A. Dehaut, I. Paul-Pont, C. Lacroix, R. Jezequel, P. Soudant and G. Duflos, Occurrence and Effects of Plastic Additives on Marine Environments and Organisms: A Review, *Chemosphere*, 2017, **182**, 781–793.

68 S. Gaw, K. V. Thomas and T. H. Hutchinson, Sources, Impacts and Trends of Pharmaceuticals in the Marine and Coastal Environment, *Philos. Trans. R. Soc., B*, 2014, 369.

69 S. D. Forestieri, K. A. Moore, R. Martinez Borrero, A. Wang, M. D. Stokes and C. D. Cappa, Temperature and Composition Dependence of Sea Spray Aerosol Production, *Geophys. Res. Lett.*, 2018, **45**, 7218–7225.

70 M. T. Leu, R. S. Timonen, L. F. Keyser and Y. L. Yung, Heterogeneous Reactions of $HNO_3(g) + NaCl(s) \rightarrow HCl(g) + NaNO_3(s)$ and $N_2O_5(g) + NaCl(s) \rightarrow ClNO_2(g) + NaNO_3(S)$, *J. Phys. Chem.*, 1995, **99**, 13203–13212.

71 E. E. Gard, M. J. Kleeman, D. S. Gross, L. S. Hughes, J. O. Allen, B. D. Morrical, D. P. Fergenson, T. Dienes, M. E. Gälli, R. J. Johnson, G. R. Cass and K. A. Prather, Direct Observation of Heterogeneous Chemistry in the Atmosphere, *Science*, 1998, **279**, 1184–1187.

72 A. P. Ault, T. L. Guasco, J. Baltrusaitis, O. S. Ryder, J. V. Trueblood, D. B. Collins, M. J. Ruppel, L. A. Cuadra-Rodriguez, K. A. Prather and V. H. Grassian, Heterogeneous Reactivity of Nitric Acid with Nascent Sea Spray Aerosol: Large Differences Observed between and within Individual Particles, *J. Phys. Chem. Lett.*, 2014, **5**, 2493–2500.

73 R. Ciuraru, L. Fine, M. Van Pinxteren, B. D'Anna, H. Herrmann and C. George, Unravelling New Processes at Interfaces: Photochemical Isoprene Production at the Sea Surface, *Environ. Sci. Technol.*, 2015, **49**, 13199–13205.

74 S. Kameyama, H. Tanimoto, S. Inomata, K. Suzuki, D. D. Komatsu, A. Hirota, U. T. A. Konno and U. Tsunogai, Application of PTR-MS to an Incubation Experiment of the Marine Diatom Thalassiosira Pseudonana, *Geochem. J.*, 2011, **45**, 355–363.

75 G. A. Novak and T. H. Bertram, Reactive VOC Production from Photochemical and Heterogeneous Reactions Occurring at the Air-Ocean Interface, *Acc. Chem. Res.*, 2020, **53**, 1014–1023.

76 K. K. Ray, H. D. Lee, M. A. Gutierrez, F. J. Chang and A. V. Tivanski, Correlating 3D Morphology, Phase State, and Viscoelastic Properties of Individual Substrate-Deposited Particles, *Anal. Chem.*, 2019, **91**, 7621–7630.

77 L. R. Pomeroy, P. J. B. le Williams, F. Azam and J. E. Hobbie, *The Microbial Loop. Oceanography*, 2007, **20**, 28–33.

78 F. Azam, T. Fenchel, J. Field, J. Gray, L. Meyer-Reil and F. Thingstad, The Ecological Role of Water-Column Microbes in the Sea, *Mar. Ecol.: Prog. Ser.*, 1983, **10**, 257–263.

79 K. B. Ksionzek, O. J. Lechtenfeld, S. L. McCallister, P. Schmitt-Kopplin, J. K. Geuer, W. Geibert and B. P. Koch, Dissolved Organic Sulfur in the Ocean: Biogeochemistry of a Petagram Inventory, *Science*, 2016, **354**, 456–459.

80 J. V. Trueblood, M. R. Alves, D. Power, M. V. Santander, R. E. Cochran, K. A. Prather and V. H. Grassian, Shedding Light on Photosensitized Reactions within Marine-Relevant Organic Thin Films, *ACS Earth Space Chem.*, 2019, **3**, 1614–1623.

81 C. D. O'Dowd, M. C. Facchini, F. Cavalli, D. Ceburnis, M. Mircea, S. Decesari, S. Fuzzi, J. Y. Young and J. P. Putaud, Biogenically Driven Organic Contribution to Marine Aerosol, *Nature*, 2004, **431**, 676–680.

82 A. D. Estillore, H. S. Morris, V. W. Or, H. D. Lee, M. R. Alves, M. A. Marciano, O. Laskina, Z. Qin, A. V. Tivanski and V. H. Grassian, Linking Hygroscopicity and the Surface Microstructure of Model Inorganic Salts, Simple and Complex Carbohydrates, and Authentic Sea Spray Aerosol Particles, *Phys. Chem. Chem. Phys.*, 2017, **19**, 21101–21111.

83 E. Saukko, A. T. Lambe, P. Massoli, T. Koop, J. P. Wright, D. R. Croasdale, D. A. Pedernera, T. B. Onasch, A. Laaksonen, P. Davidovits, D. R. Worsnop and A. Virtanen, Humidity-Dependent Phase State of SOA Particles from Biogenic and Anthropogenic Precursors, *Atmos. Chem. Phys.*, 2012, **12**, 7517–7529.

84 A. Athanasiadis, C. Fitzgerald, N. M. Davidson, C. Giorio, S. W. Botchway, A. D. Ward, M. Kalberer, F. D. Pope and M. K. Kuimova, Dynamic Viscosity Mapping of the Oxidation of Squalene Aerosol Particles, *Phys. Chem. Chem. Phys.*, 2016, **18**, 30385–30393.

85 S. Shen, P. A. Jaques, Y. Zhu, M. D. Geller and C. Sioutas, Evaluation of the SMPS-APS System as a Continuous

Monitor for Measuring PM2.5, PM10 and Coarse (PM2.5–10) Concentrations, *Atmos. Environ.*, 2002, **36**, 3939–3950.

86 T. M. Peters and D. Leith, Concentration Measurement and Counting Efficiency of the Aerodynamic Particle Sizer 3321, *J. Aerosol Sci.*, 2003, **34**, 627–634.

87 X. F. Lopez-Yglesias, M. C. Yeung, S. E. Dey, F. J. Brechtel and C. K. Chan, Performance Evaluation of the Brechtel Mfg. Humidified Tandem Differential Mobility Analyzer (BMI HTDMA) for Studying Hygroscopic Properties of Aerosol Particles, *Aerosol Sci. Technol.*, 2014, **48**, 969–980.

88 S. V. Hering, G. S. Lewis, S. R. Spielman and A. Eiguren-Fernandez, A MAGIC Concept for Self-Sustained, Water-Based, Ultrafine Particle Counting, *Aerosol Sci. Technol.*, 2019, **53**, 63–72.

89 E. Gard, J. E. Mayer, B. D. Morrical, T. Dienes, D. P. Fergenson and K. a. Prather, Real-Time Analysis of Individual Atmospheric Aerosol Particles: Design and Performance of a Portable ATOFMS, *Anal. Chem.*, 1997, **69**, 4083–4091.

90 D. Voisin, J. N. Smith, H. Sakurai, P. H. McMurry and F. L. Eisele, Thermal Desorption Chemical Ionization Mass Spectrometer for Ultrafine Particle Chemical Composition, *Aerosol Sci. Technol.*, 2003, **37**, 471–475.

91 J. N. Smith, K. F. Moore, P. H. McMurry and F. L. Eisele, Atmospheric Measurements of Sub-20 Nm Diameter Particle Chemical Composition by Thermal Desorption Chemical Ionization Mass Spectrometry, *Aerosol Sci. Technol.*, 2004, **38**, 100–110.

92 F. D. Lopez-Hilfiker, V. Pospisilova, W. Huang, M. Kalberer, C. Mohr, G. Stefenelli, J. A. Thornton, U. Baltensperger, A. S. H. Prevot and J. G. Slowik, An Extractive Electrospray Ionization Time-of-Flight Mass Spectrometer (EESI-TOF) for Online Measurement of Atmospheric Aerosol Particles, *Atmos. Meas. Tech.*, 2019, **12**, 4867–4886.

93 G. C. Roberts and A. Nenes, A Continuous-Flow Streamwise Thermal-Gradient CCN Chamber for Atmospheric Measurements, *Aerosol Sci. Technol.*, 2005, **39**, 206–221.

94 S. Jain and G. A. Petrucci, A New Method to Measure Aerosol Particle Bounce Using a Cascade Electrical Low Pressure Impactor, *Aerosol Sci. Technol.*, 2015, **49**, 390–399.

95 P. J. Demott, A. J. Prenni, G. R. McMeeking, R. C. Sullivan, M. D. Petters, Y. Tobo, M. Niemand, O. Möhler, J. R. Snider, Z. Wang and S. M. Kreidenweis, Integrating Laboratory and Field Data to Quantify the Immersion Freezing Ice Nucleation Activity of Mineral Dust Particles, *Atmos. Chem. Phys.*, 2015, **15**, 393–409.

96 A. M. Gabey, W. R. Stanley, M. W. Gallagher and P. H. Kaye, The Fluorescence Properties of Aerosol Larger than 0.8 μ in Urban and Tropical Rainforest Locations, *Atmos. Chem. Phys.*, 2011, **11**, 5491–5504.

97 R. J. Perkins, S. M. Gillette, T. C. J. Hill and P. J. Demott, The Labile Nature of Ice Nucleation by Arizona Test Dust, *ACS Earth Space Chem.*, 2020, **4**, 133–141.

98 R. E. Cochran, O. Laskina, T. Jayarathne, A. Laskin, J. Laskin, P. Lin, C. Sultana, C. Lee, K. A. Moore, C. D. Cappa, T. H. Bertram, K. A. Prather, V. H. Grassian and E. A. Stone, Analysis of Organic Anionic Surfactants in Fine and Coarse Fractions of Freshly Emitted Sea Spray Aerosol, *Environ. Sci. Technol.*, 2016, **50**, 2477–2486.

99 A. P. S. Hettiyadura, T. Jayarathne, K. Baumann, A. H. Goldstein, J. A. De Gouw, A. Koss, F. N. Keutsch, K. Skog and E. A. Stone, Qualitative and Quantitative Analysis of Atmospheric Organosulfates in Centreville, Alabama, *Atmos. Chem. Phys.*, 2017, **17**, 1343–1359.

100 H. D. Lee, K. K. Ray and A. V. Tivanski, Solid, Semisolid, and Liquid Phase States of Individual Submicrometer Particles Directly Probed Using Atomic Force Microscopy, *Anal. Chem.*, 2017, **89**, 12720–12726.

101 V. W. Or, A. D. Estillore, A. V. Tivanski and V. H. Grassian, Lab on a Tip: Atomic Force Microscopy-Photothermal Infrared Spectroscopy of Atmospherically Relevant Organic/Inorganic Aerosol Particles in the Nanometer to Micrometer Size Range, *Analyst*, 2018, **143**, 2765–2774.

102 L. E. Mael, H. Busse and V. H. Grassian, Measurements of Immersion Freezing and Heterogeneous Chemistry of Atmospherically Relevant Single Particles with Micro-Raman Spectroscopy, *Anal. Chem.*, 2019, **91**, 11138–11145.

103 K. J. Angle, D. R. Crocker, R. M. C. Simpson, K. J. Mayer, L. A. Garofalo, A. N. Moore, S. L. Mora Garcia, V. W. Or, S. Srinivasan, M. Farhan, J. S. Sauer, C. Lee, M. A. Pothier, D. K. Farmer, T. R. Martz, T. H. Bertram, C. D. Cappa, K. A. Prather and V. H. Grassian, Acidity across the Interface from the Ocean Surface to Sea Spray Aerosol, *Proc. Natl. Acad. Sci. U. S. A.*, 2021, **118**, 1–6.

104 D. Petras, I. Koester, R. Da Silva, B. M. Stephens, A. F. Haas, C. E. Nelson, L. W. Kelly, L. I. Aluwihare and P. C. Dorrestein, High-Resolution Liquid Chromatography Tandem Mass Spectrometry Enables Large Scale Molecular Characterization of Dissolved Organic Matter, *Front. Mar. Sci.*, 2017, **4**, 405.

105 H. G. Hoppe, Significance of Exoenzymatic Activities in the Ecology of Brackish Water: Measurements by Means of Methylumbelliferyl-Substrates, *Mar. Ecol.: Prog. Ser.*, 1983, **11**, 299–308.

106 D. R. Crocker, R. E. Hernandez, H. D. Huang, M. A. Pendergraft, R. Cao, J. Dai, C. K. Morris, G. B. Deane, K. A. Prather and M. H. Thiemens, Biological Influence on 13C and Organic Composition of Nascent Sea Spray Aerosol, *ACS Earth Space Chem.*, 2020, **4**, 1686–1699.

107 Y. Wei, Y. Jiao, D. An, D. Li, W. Li and Q. Wei, Review of Dissolved Oxygen Detection Technology: From Laboratory Analysis to Online Intelligent Detection, *Sensors*, 2019, 19.

108 W. Walters, E. R. Hyde, D. Berg-Lyons, G. Ackermann, G. Humphrey, A. Parada, J. A. Gilbert, J. K. Jansson, J. G. Caporaso, J. A. Fuhrman, A. Apprill and R. Knight, Improved Bacterial 16S RRNA Gene (V4 and V4-5) and Fungal Internal Transcribed Spacer Marker Gene Primers for Microbial Community Surveys, *mSystems*, 2016, **1**, e00009–e00015.

109 U. Christaki, C. Courties, R. Massana, P. Catala, P. Lebaron, J. M. Gasol and M. V. Zubkov, Optimized Routine Flow Cytometric Enumeration of Heterotrophic Flagellates

Using SYBR Green I, *Limnol. Oceanogr.: Methods*, 2011, **9**, 329–339.

110 J. J. Minich, Q. Zhu, S. Janssen, R. Hendrickson, A. Amir, R. Vetter, J. Hyde, M. M. Doty, K. Stillwell, J. Benardini, J. H. Kim, E. E. Allen, K. Venkateswaran and R. Knight, KatharoSeq Enables High-Throughput Microbiome Analysis from Low-Biomass Samples, *mSystems*, 2018, **3**(3), e00218-17.

111 A. Stubbins and T. Dittmar, Low Volume Quantification of Dissolved Organic Carbon and Dissolved Nitrogen, *Limnol. Oceanogr.: Methods*, 2012, **10**, 347–352.

112 S. Becker, M. Aoyama, E. M. S. Woodward, K. Bakker, S. Coverly, C. Mahaffey and T. Tanhua, GO-SHIP Repeat Hydrography Nutrient Manual: The Precise and Accurate Determination of Dissolved Inorganic Nutrients in Seawater, Using Continuous Flow Analysis Methods, *Front. Mar. Sci.*, 2020, 7.

113 B. Hales, D. Chipman and T. Takahashi, High-Frequency Measurement of Partial Pressure and Total Concentration of Carbon Dioxide in Seawater Using Microporous Hydrophobic Membrane Contactors, *Limnol. Oceanogr.: Methods*, 2004, **2**, 356–364.

114 D. Smith and F. Azam, A Simple, Economical Method for Measuring Bacterial Protein Synthesis Rates in Seawater Using 3H-Leucine, *Mar. Microb. Food Webs*, 1992, **6**, 107–114.

115 J. Dinasquet, M. Tiirola and F. Azam, Enrichment of Bacterioplankton Able to Utilize One-Carbon and Methylated Compounds in the Coastal Pacific Ocean, *Front. Mar. Sci.*, 2018, **5**, 307.

116 E. C. Asher, J. W. H. Dacey, T. Jarniková and P. D. Tortell, Measurement of DMS, DMSO, and DMSP in Natural Waters by Automated Sequential Chemical Analysis, *Limnol. Oceanogr.: Methods*, 2015, **13**, 451–462.

117 N. M. Levine, V. A. Varaljay, D. A. Toole, J. W. H. Dacey, S. C. Doney and M. A. Moran, Environmental, Biochemical and Genetic Drivers of DMSP Degradation and DMS Production in the Sargasso Sea, *Environ. Microbiol.*, 2012, **14**, 1210–1223.

118 T. Gherman, D. S. Venables, S. Vaughan, J. Orphal and A. A. Ruth, Incoherent Broadband Cavity-Enhanced Absorption Spectroscopy in the near-Ultraviolet: Application to HONO and NO_2, *Environ. Sci. Technol.*, 2008, **42**, 890–895.

